J. Fluid Mech. (1985), *vol.* 157, *pp.* 225–263
Printed in Great Britain

Nonlinear Kelvin–Helmholtz instability of a finite vortex layer

By C. POZRIKIDIS AND J. J. L. HIGDON
Department of Chemical Engineering, University of Illinois,
1209 W California Street, Urbana, Illinois 61801

(Received 28 June 1984 and in revised form 15 February 1985)

The nonlinear growth of periodic disturbances on a finite vortex layer is examined. Under the assumption of constant vorticity, the evolution of the layer may be analysed by following the contour of the vortex region. A numerical procedure is introduced which leads to higher-order accuracy than previous methods with negligible increase in computational effort. The response of the vortex layer is studied as a function of layer thickness and the amplitude and form of the initial disturbance. For small initial disturbances, all unstable layers form a large rotating vortex core of nearly elliptical shape. The growth rate of the disturbances is strongly affected by the layer thickness; however, the final amplitude of the disturbance is relatively insensitive to the thickness and reaches a maximum value of approximately 20 % of the wavelength. In the fully developed layers, the amplitude shows a small oscillation owing to the rotation of the vortex core. For finite-amplitude initial disturbances, the evolution of the layer is a function of the initial amplitude. For thin layers with thickness less than 3 % of the wavelength, three different patterns were observed in the vortex-core region: a compact elliptic core, an elongated S-shaped core and a bifurcation into two orbiting cores. For thicker layers, stationary elliptic cores may develop if the thickness exceeds 15 % of the wavelength. The spacing and eccentricity of these cores is in good agreement with previously discovered steady-state solutions. The growth rate of interfacial area (or length of the vortex contour) is calculated and is found to approach a constant value in well-developed vortex layers.

1. Introduction

A variety of fluid flows are characterized by regions where a sharp change in the velocity occurs over a thin layer of the fluid. The two major classes of such flows are boundary layers on solid surfaces and free shear layers in the fluid. Free shear layers arise in natural flows in the atmosphere and in the oceans, as well as in industrial processes involving the mixing of fluid streams. Perhaps, most importantly, they are fundamental to an understanding of the dynamics of flow at high Reynolds number.

Free shear layers have received special attention in recent years owing to the widespread interest in coherent structures in turbulent flow. There has grown up around the subject a vast literature of experimental and theoretical studies. The chief goal of these efforts has been to describe the detailed structure of the layers, to predict the growth rate and to determine the effect of the relevant flow parameters. A comprehensive review of the major efforts in this area has been given recently by Ho & Huerre (1984). Both laminar and turbulent shear layers have been studied using a variety of techniques. These include turbulence modelling, numerical solutions of

the Navier–Stokes equations, inviscid models based on vortex dynamics and both linear and nonlinear stability analysis.

In the study of purely inviscid shear layers, one of the most promising approaches is through the formalism of vortex dynamics. The major efforts in this area may be classified according to the distribution of vorticity. In the first class, the shear layer is represented by a large collection of discrete vortex markers. The induced velocity is calculated directly from the distribution of point vortices or vortex cores, or indirectly through the cloud-in-cell method. These methods provide an adequate description of the layer in an average sense, but cannot resolve the finer details of the motion, except at prohibitive cost. Representative calculations include Acton (1976), Ashurst (1979), Aref & Siggia (1980) and Krasny (1984). The second class of vortex methods considers the shear layer in the asymptotic limit as a vortex sheet. This method is subject to severe mathematical difficulties, owing to the appearance of singularities in the description of the sheet. Recent papers dealing with periodic disturbances on infinite sheets include Meiron, Baker & Orszag (1982) and Higdon & Pozrikidis (1985). In the third class of vortex methods, the vorticity is bounded and is distributed over finite regions of the fluid. In the simplest case, the vorticity is assumed constant, and the problem is reduced to one of following the contours of the vortex regions. Zabusky and coworkers (see e.g. Overman & Zabusky 1982) have used this model to study isolated patches of vorticity in an infinite fluid. They have established the existence of steady-state vortex regions and have examined the coalescence of neighbouring vortex cores. Pullin (1981) used the model to study periodic disturbances on a vortex layer attached to a wall. A review of the applications of all types of vortex methods to free shear layers has been given by Aref (1983).

In the present paper, we use the constant-vorticity model to study the growth of periodic disturbances on free shear layers. Our goal is to investigate the effect of the layer thickness on the growth of disturbances. Linear stability theory, Rayleigh (1880) (also see Appendix), shows that the maximum growth rate occurs for wavelengths approximately 8 times the layer thickness, while wavelengths shorter than 5 layer thicknesses are stable. We shall study the effect of thickness on the growth rate for nonlinear disturbances. In addition, we shall show that, for finite-amplitude disturbances, not only the thickness of the layer, but also the form of the initial disturbance affect the asymptotic structure of the layer.

2. Mathematical formulation

2.1. *Calculation of the fluid velocity*

A basic theorem of vector analysis states that any vector field may be separated into two parts, one of which has zero divergence and the other zero curl. In fluid dynamics, we extend this theorem to write the velocity as the sum of three contributions: the first due to the vorticity, the second due to the local expansion of the fluid and the third due to a velocity potential. For an incompressible, unbounded fluid, the last two are zero, and we may write the velocity simply as an integral over the vorticity distribution.

In two dimensions,

$$q^* = u - \mathrm{i}v = -\int \frac{\mathrm{d}W}{\mathrm{d}z'} \omega(z')\, \mathrm{d}S(z'), \tag{1}$$

where q^* is the complex velocity, ω is the vorticity and $W(z')$ is the complex potential for a point vortex, defined as

$$W(z') = \phi + \mathrm{i}\psi = \frac{1}{2\pi\mathrm{i}} \ln (z - z'). \tag{2}$$

The integral expression in (1) may be used to evaluate the velocity at any point in the fluid. Thus, we might calculate the velocity of all elements of rotational fluid and follow the evolution of the vortex layer in time. Before we can implement such a strategy, we require a measure of the rate at which vorticity changes over time. For constant-density or barotropic fluids in two-dimensional motion, Kelvin's theorem guarantees that the vorticity of an element of fluid is conserved. Therefore the vorticity moves with the fluid, and we may find the vorticity at any instant by following the trajectory of material points in the vortex layer.

With the additional assumption that the vorticity is initially uniform, the calculation may be greatly simplified. Converting to real variables, we employ the streamfunction ψ and apply Green's theorm to (1) to obtain

$$\boldsymbol{u} = \omega \int_C \psi \boldsymbol{t} \, \mathrm{d}l, \tag{3}$$

where C represents all contours bounding the vortex region and $\boldsymbol{t}$ is the unit vector tangent to C.

As an alternative, we might use the velocity potential ϕ and apply Gauss' theorem to (1) yielding

$$\boldsymbol{u} = -\omega \int_C \phi \boldsymbol{n} \, \mathrm{d}l, \tag{4}$$

where $\boldsymbol{n}$ is the unit normal vector.

With the velocity defined by (3) or (4), we have a nonlinear integro-differential equation for the motion of material points on the vorticity contours. While a few simple solutions have been found (e.g. Kirchoff 1876), one must resort to numerical techniques to study more general configurations. In a standard numerical procedure, the vortex contour is identified by a finite number of marker points. The contour integrals are evaluated by choosing a suitable interpolating function, and the velocity of each marker point is calculated. The positions of the marker points are updated and the calculation steps forward in time using standard algorithms.

Previous authors including Zabusky and coworkers (Deem & Zabusky 1978; Zabusky, Hughes & Roberts 1979; Overman & Zabusky 1982) and Pullin (1981) have used straight-line segments to interpolate between marker points. In the present study, we employ a higher-order discretization, fitting circular arcs through neighbouring sets of points. This choice gives higher accuracy, allows for the analytical evaluation of the integrals on each interval and requires no more computational effort than the straight-segment representation. Although either (3) or (4) may be used to calculate the velocity, we find it more convenient to work with the stream function, because the velocity potential is multivalued.

For infinite vortex layers with periodic disturbances, we do not use (1) or (3) directly because of the infinite interval of integration. Instead, the complex potential (2) is replaced by the potential for a periodic line of vortex singularities

$$W_{\mathrm{P}}(z') = \phi_{\mathrm{P}} + \mathrm{i}\psi_{\mathrm{P}} = \frac{1}{2\pi\mathrm{i}} \ln \left[\sin \frac{\pi(z - z')}{\lambda} \right] \tag{5}$$

(see e.g. Lamb 1932, §156).

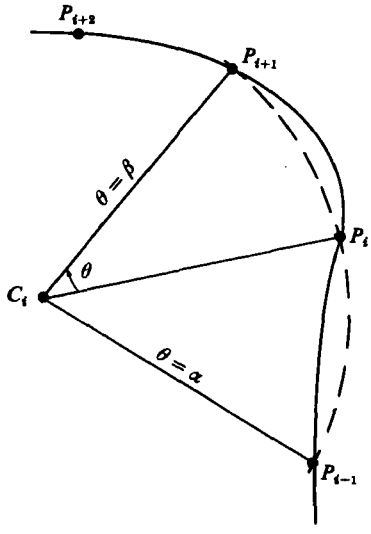

FIGURE 1. Local representation of vortex contour with circular arc.

Similarly, the stream function ψ in (3) is replaced by its periodic counterpart ψ_{P} defined as the imaginary part of (5). With this substitution, we find that we can no longer evaluate the integrals on each discrete interval analytically. To circumvent this difficulty, we subtract from the integrand the stream function for a single-vortex singularity. The remainder is non-singular and may be easily evaluated using standard quadratures. This procedure is quite common and is similar to that employed by Pullin (1981). Thus, we write the velocity in the form

$$\boldsymbol{u} = \omega \int_{C_\lambda} \psi \boldsymbol{t}\, \mathrm{d}l + \omega \int_{C_\lambda} (\psi_{\mathrm{P}} - \psi)\, \boldsymbol{t}\, \mathrm{d}l, \tag{6}$$

where the integration extends over the contour C_λ bounding a single period of the vortex layer.

In this expression, the first integral is evaluated analytically over each arc, while the second integral is evaluated numerically. In practice, a five-point Gauss–Legendre quadrature on each interval is sufficient to make the numerical error smaller than the discretization error.

2.2. *Error analysis*

To estimate the error involved in our discretization, we consider a small section of the sheet passing through three consecutive points as shown in figure 1. In a local polar coordinate system with the origin at the centre of the arc, the exact position of the contour is specified by

$$r = R(1+f(\theta)), \tag{7}$$

where R is the radius of the arc.

With the requirement that the contour pass through the three specified points, we may write

$$f(\theta) = \theta(\theta-\alpha)\,(\theta-\beta)\,g(\theta), \tag{8}$$

where $g(\theta)$ is a non-singular function of θ; α and β are the angles subtended by the outer points. Approximating the contour with a circular arc is equivalent to setting $f(\theta)$ identically equal to zero.

With the definitions above, the integral over the arc takes the form

$$\boldsymbol{u} = \frac{R}{4\pi}\int_{\alpha}^{\beta} \ln\left[R^2(4(1+f)\sin^2\tfrac{1}{2}\theta + f^2)\right]\left[f'\boldsymbol{e}_r + (1+f)\boldsymbol{e}_\theta\right]\mathrm{d}\theta. \tag{9}$$

The error involved in the discretization may be found by expanding the integrand with respect to θ, evaluating and comparing with the case $f = 0$. We find

$$\boldsymbol{u}_{\text{exact}} = \boldsymbol{u}_{\text{approx}}(1 + O(\epsilon^3)), \tag{10}$$

where $\boldsymbol{u}_{\text{approx}}$ represents the arc discretization and $\epsilon = \max(\alpha, \beta)$.

A similar analysis applied to the straight-segment discretization gives an error of order ϵ^2. In this case, ϵ is the length of the segment multiplied by the local curvature of the sheet.

2.3. *Numerical procedure*

The method for evaluating the fluid velocity described above forms the foundation of our calculations. To implement this procedure in numerical computations, we identify a collection of marker points on the initial contour. The initial velocity of each point is calculated and the computation moves forward one step. At each successive instant, the distribution of points is examined and new points are inserted according to two criteria. If the arc subtended by any trio of points exceeds a pre-established maximum, additional points are inserted using the method suggested by Higdon & Pozrikidis (1985). Briefly, this involves placing the new points in positions such that the curvature remains a smooth function of arclength. The second criterion is that the length of an arc should not exceed a given maximum length. While the length of the arcs does not directly affect the accuracy of the velocity calculation, this second requirement leads to a more uniform rate of point insertion. Finally, when a large number of points accumulates in a region of small curvature, i.e. where only a few are needed for an accurate velocity calculation, points are eliminated to minimize computation time.

For the calculations presented in the following section, a 4th-order Runge–Kutta method was used for the time integration. In certain cases, this was combined with Gear's (1971) method to adjust the time step to optimize computational efficiency. A typical calculation for a single layer required approximately 10 min CPU time on a CYBER 175 or 3 h on a VAX 11/780. The criteria for point insertion and time step were established empirically. The number of marker points used in each calculation is indicated on the respective figures in the following section. In a typical case, 150 marker points were used in the final step of the calculation. The accuracy of the calculations was verified by repeating selected calculations with twice the number of marker points and half the time step. In all cases, the profiles were identical to within a plotted line width.

3. Periodic disturbances on finite vortex layers

3.1. *Specification of the initial disturbance*

Having developed an efficient procedure for following the evolution of finite vortex layers, we consider the specific problem of layers with periodic disturbances. We specify the initial perturbation of the boundaries in the form

$$\left.\begin{aligned} y^+ &= \tfrac{1}{2}b + \alpha_0 \sin(kx - \tfrac{1}{2}\phi), \\ y^- &= -\tfrac{1}{2}b + \alpha_0 \sin(kx + \tfrac{1}{2}\phi), \end{aligned}\right\} \tag{11}$$

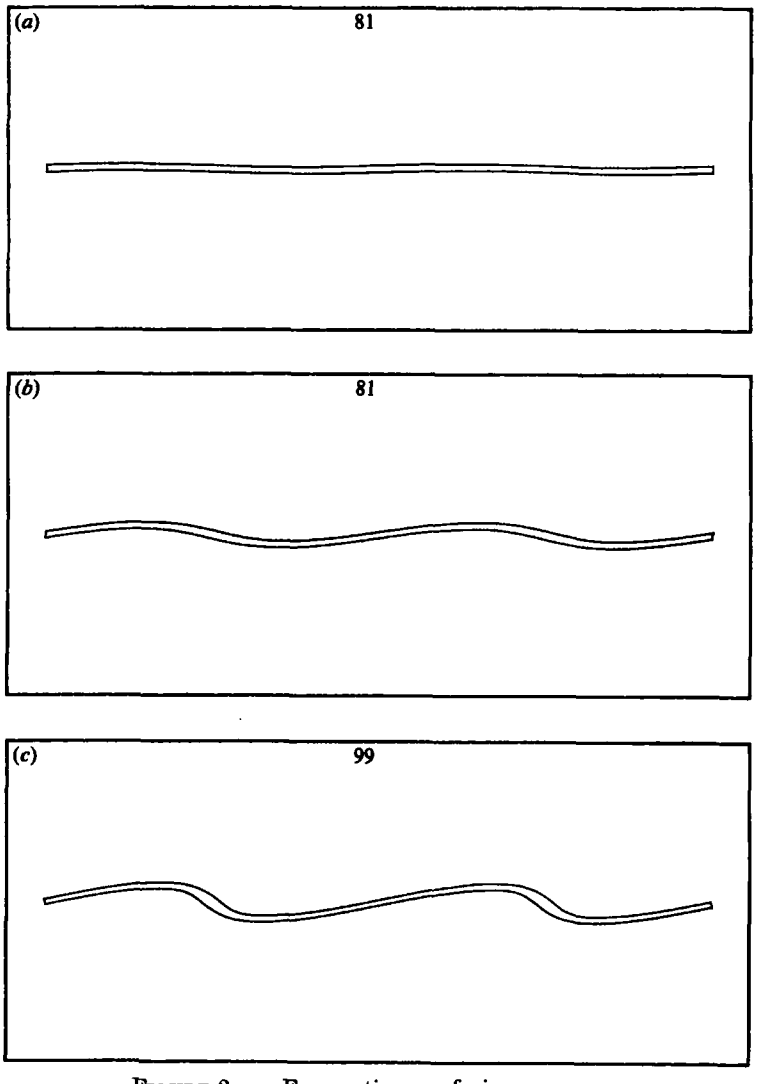

FIGURE 2 *a–c*. For caption see facing page.

where b is the thickness of the layer, k is the wavenumber, α_0 is the initial amplitude, and ϕ is the phase shift between the upper and lower boundaries. When $\phi = 0$, the mean position of the layer is perturbed, but the total circulation per unit length is constant; we refer to this as a shape disturbance. Similarly, when $\phi = \pi$, the circulation is perturbed, but the mean position of the layer is undisturbed; hence we call this a circulation disturbance. The complete specification of the initial disturbance in non-dimensional form requires values for kb, $\alpha_0 k$ and ϕ. We shall follow the evolution of the layers in terms of the non-dimensional time $t' = \omega t$.

The phase angle ϕ dictates the type of the initial disturbance. The two disturbances identified above as shape and circulation are the most natural from a physical point of view; however, any value of ϕ from $-\pi$ to π is certainly possible. An obvious choice is the phase shift associated with the growing normal mode in the linear stability analysis. The value of ϕ for this normal mode changes as a function of thickness, ranging from $\phi = 0$ for $kb = 0$ to $\phi = \pi$ for $kb = 1.278^{+}$, the maximum thickness for which linear theory predicts the growth of disturbances.

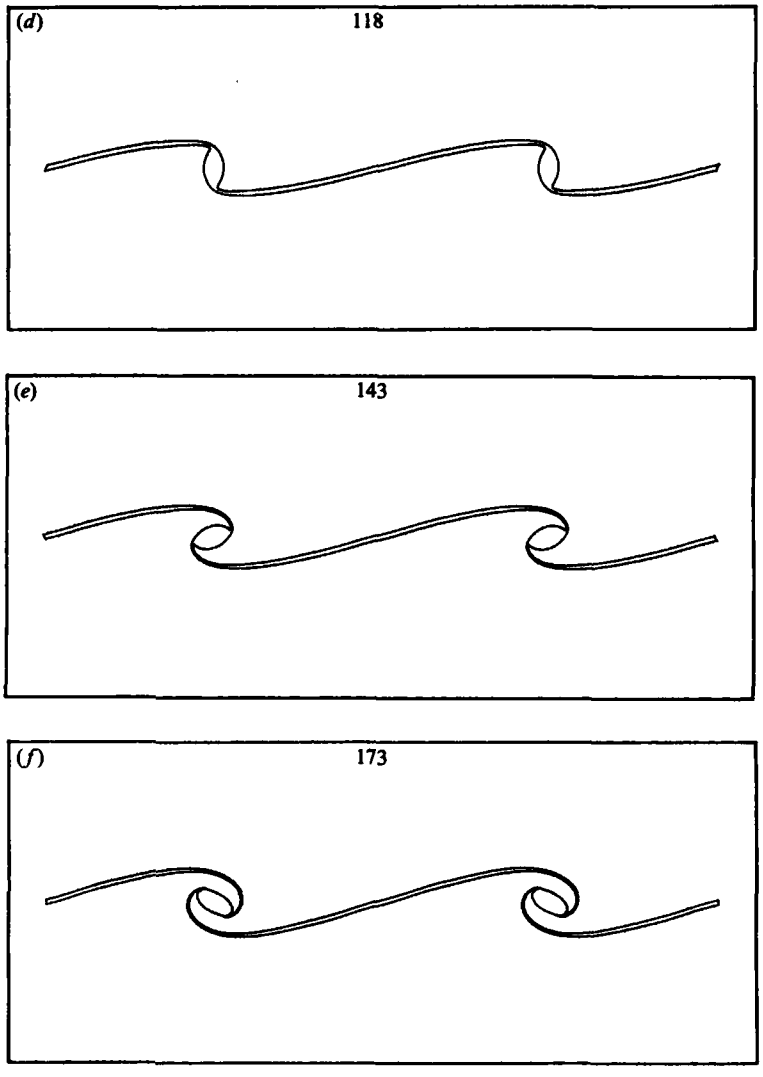

FIGURE 2. Evolution of vortex layer subject to small-amplitude shape disturbance, $\alpha_0 k = 0.03$; layer thickness, $kb = 0.125$. Numbers at top of this and subsequent figures are the number of marker points along the contour. (*a*) $t' = 0$; (*b*) 42.5; (*c*) 53.0; (*d*) 60.5; (*e*) 65.0; (*f*) 69.2.

3.2. *Shape disturbances – small amplitude*

To isolate the effect of layer thickness for disturbances of fixed phase, we start by considering small disturbances with $\phi = 0$, i.e. shape disturbances. All perturbations studied in this section begin with an initial amplitude $\alpha_0 k = 0.03$. Calculations show that the initial development for this amplitude is well described by linear theory; hence smaller amplitudes are unnecessary. Figure 2 shows the evolution of a shape disturbance on a thin vortex layer with $kb = 0.125$. This corresponds to a layer thickness approximately 0.02 times the wavelength. The initial view, figure 2(*a*), shows the almost imperceptible initial disturbance. Figure 2(*b*) shows the shape of the layer after the first phase of the evolution which is well described by linear theory. The boundaries of the layer are nearly sine waves and show only a slight shift in phase. This phase shift is predicted by linear theory, because the growing normal mode has a small non-zero phase shift for this thickness. Figure 2(*c*) shows the first signs of

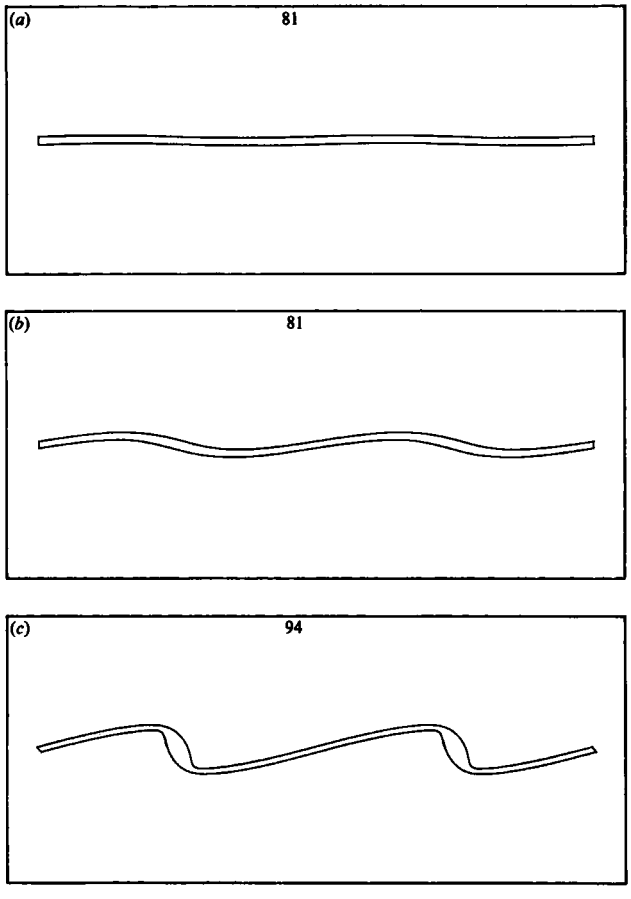

FIGURE 3 *a–c*. For caption see facing page.

markedly nonlinear behaviour with the accumulation of vorticity within small well-defined regions along the layer. This process continues in figure 2(*d–f*) with the formation of rotating vortex cores of nearly elliptical shape. Figure 2(*f*) represents the asymptotic form of the layer with a compact central core surrounded by long thin vortex wings. At later times, the wings will continue to spiral around the cores, but the relative distribution of vorticity between the cores and the wings will remain nearly constant. Despite the accumulation in the cores, nearly 75% of the vorticity remains in the wings for this layer.

Figure 3 shows the evolution for a layer with thickness $kb = 0.175$, slightly thicker than the previous case. This demonstrates essentially the same behaviour as the previous layer with the same stages in the development. The important difference between the two cases is that the thicker layer evolves faster owing to the greater area of vorticity, i.e. owing to the greater shear across the layer. In this sequence, the calculation has been extended to a later time to show the continuation of the roll-up process.

Proceeding to layers of substantially greater thickness, we observe the development of a $kb = 0.50$ layer in figure 4. Once again, the early stages are similar, starting with an infinitesimal initial perturbation, figure 4(*a*), a small-amplitude disturbance consistent with the predictions of linear theory in figure 4(*b*), and the appearance of

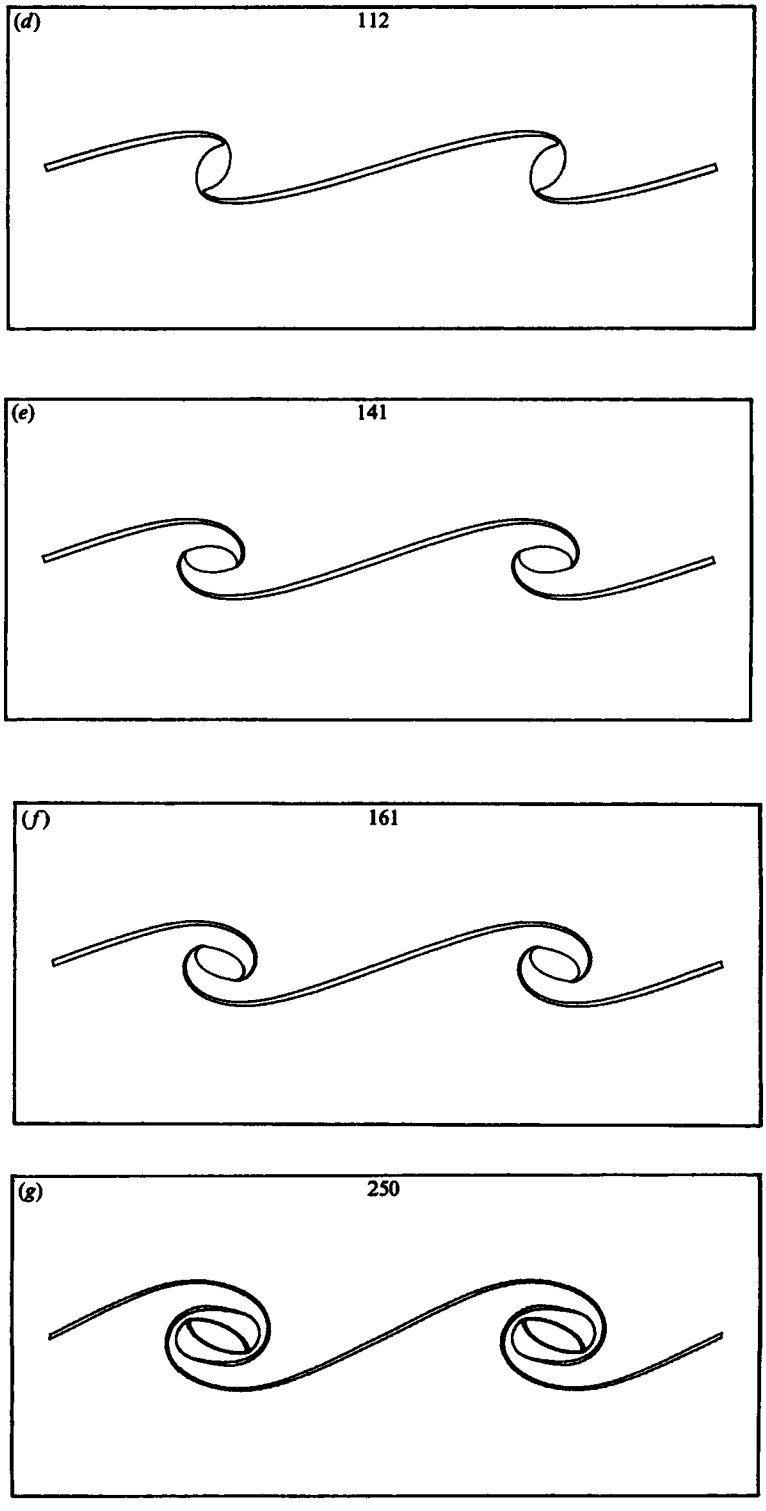

FIGURE 3. Evolution of vortex layer with small-amplitude shape disturbance; layer thickness, $kb = 0.175$. (*a*) $t' = 0$; (*b*) 33.0; (*c*) 45.0; (*d*) 49.5; (*e*) 54.0; (*f*) 55.8; (*g*) 69.8.

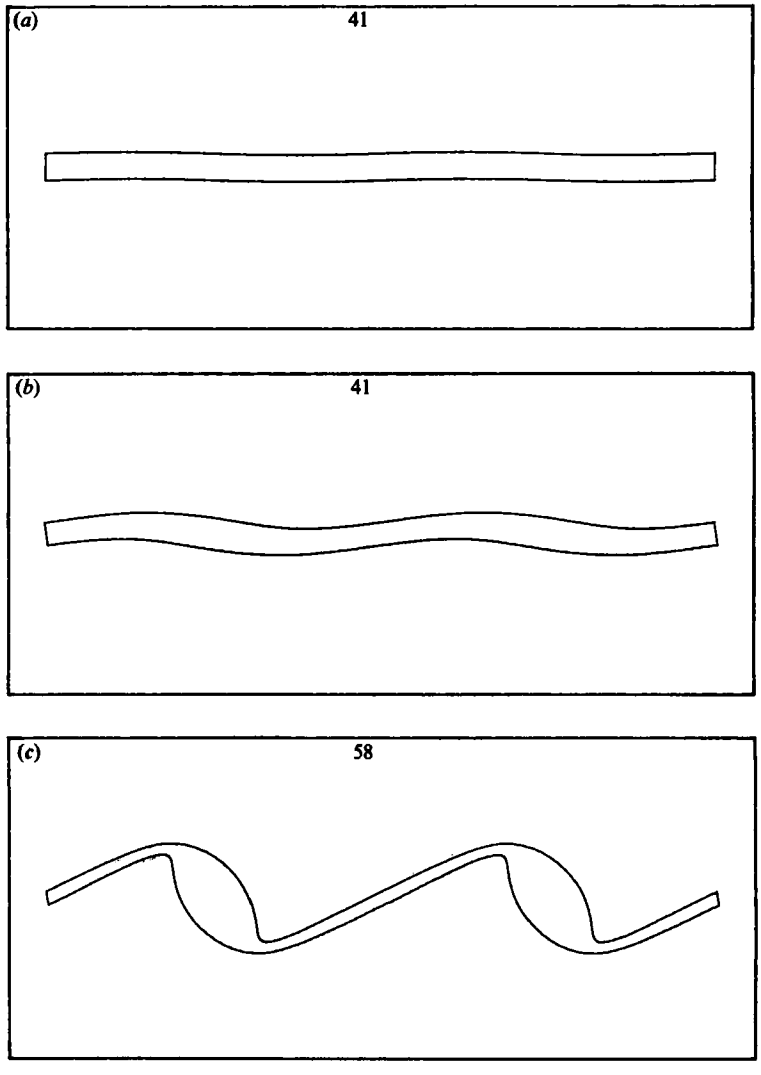

FIGURE 4 *a–c*. For caption see facing page.

nonlinear effects with the accumulation of vorticity in (figure 4(*c*). It is in the later stages, figure 4(*d–f*), that we see a qualitative difference in the roll-up process. The core is larger of course because of the greater total quantity of vorticity but, in addition, the core contains a greater fraction of the vorticity – 60% *versus* 25% for the thinnest layer $kb = 0.125$. This concentration of vorticity dominates the flow with a much stronger rotating flow in the core region. We note that the elliptical core rotates with a nearly constant angular velocity.

The evolution of a layer with still greater thickness, $kb = 1.00$, is shown in figure 5. In this case, the qualitative differences appear even at the earliest stages. Figure 5(*b*) shows the small-amplitude disturbance which may be predicted by linear theory; however, we notice a substantial phase shift between the upper and lower surfaces. Physically, this is due to the translation of the surfaces in the shear flow. From linear analysis, this may be predicted because the growing normal mode has a phase shift of $\frac{1}{2}\pi$ for this thickness. Figure 5(*c*) shows a distinctly nonlinear growth and is

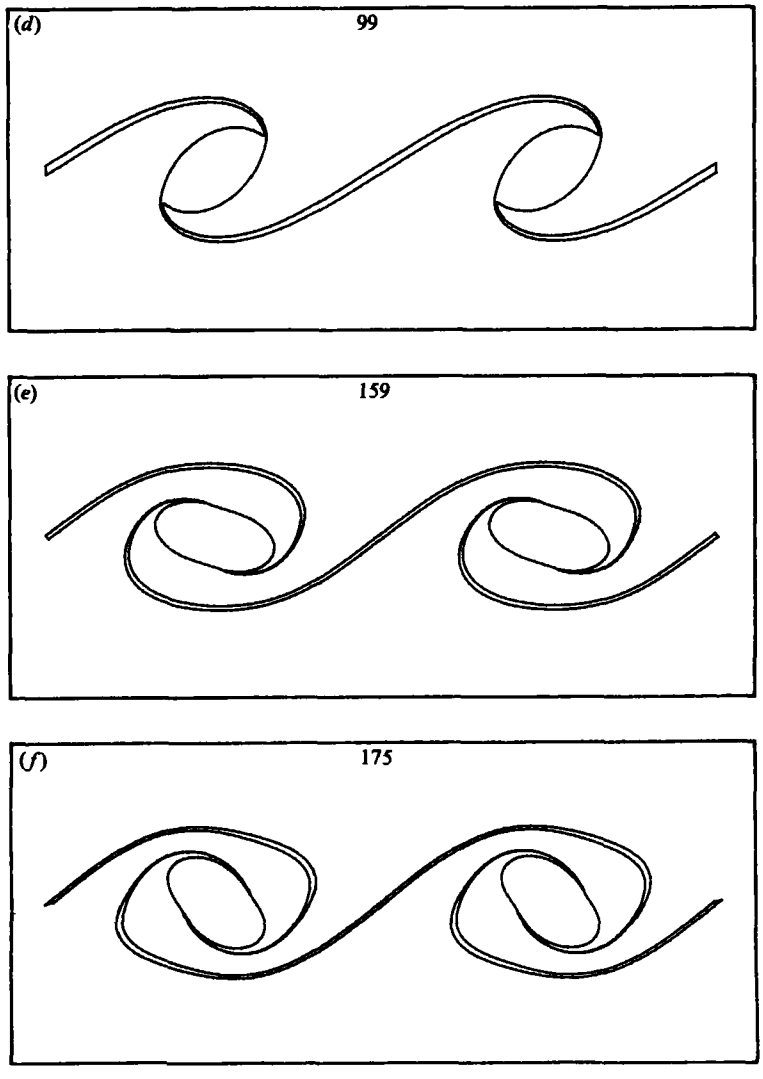

FIGURE 4. Evolution of vortex layer with small-amplitude shape disturbance; layer thickness, $kb = 0.50$. (*a*) $t' = 0$; (*b*) 13.2; (*c*) 24.0; (*d*) 29.4; (*e*) 34.8; (*f*) 37.2.

interesting because of the very rapid accumulation of vorticity in the cores. A comparison with figure 4(*c*) shows that the wings or 'braids' are actually thinner for this layer although the initial thickness was greater. This may be explained by the extreme concentration of vorticity in the core with the resulting extensional flow in the intervening region. In the succeeding stages, figure 5(*d–f*), the wings are drawn out into extremely thin lines with nearly all the vorticity, approximately 90%, concentrated in the elliptical cores. While the cores rotate with almost constant velocity as before, the angular velocity is substantially smaller than for the $kb = 0.50$ layer.

The final layer on which we consider infinitesimal shape disturbances is of thickness $kb = 1.278^{+}$. This corresponds to the point of neutral stability as predicted by linear theory. All layers of greater thickness are stable to small disturbances. As can be seen in figure 6, the disturbances grow, but the time required to reach finite amplitude,

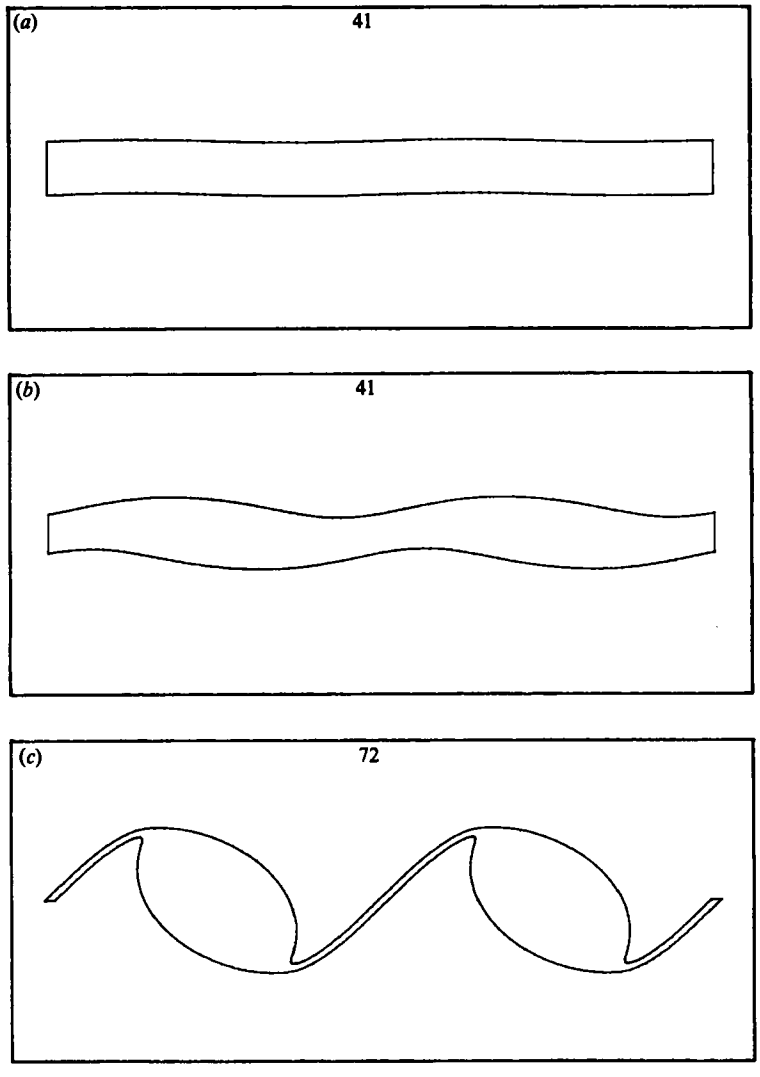

FIGURE 5 *a–c*. For caption see facing page.

figure 6 (*b*), is much greater than for the thinner layers presented earlier. In other ways, the $kb = 1.278$ layer is similar to the $kb = 1.00$ layer, with an even more pronounced accumulation of vorticity and thinner wings than in the previous case. Calculations performed for thicker layers showed no growth for infinitesimal disturbances. This is consistent with expectations from linear theory.

3.3. *Circulation disturbances – small amplitude*

We have seen that the asymptotic form of the vortex layer is strongly influenced by the thickness of the layer or equivalently by the wavelength of the disturbance. We now consider the effect of changing the form of the initial disturbance by studying the evolution of layers subject to circulation disturbances. For disturbances which are truly infinitesimal, i.e. in the limit as $\alpha_0 k \to 0$, there will be no difference in the evolving profiles, because both will emerge from the growing normal mode of linear theory. There will be differences in the initial growth rates, as discussed in a later

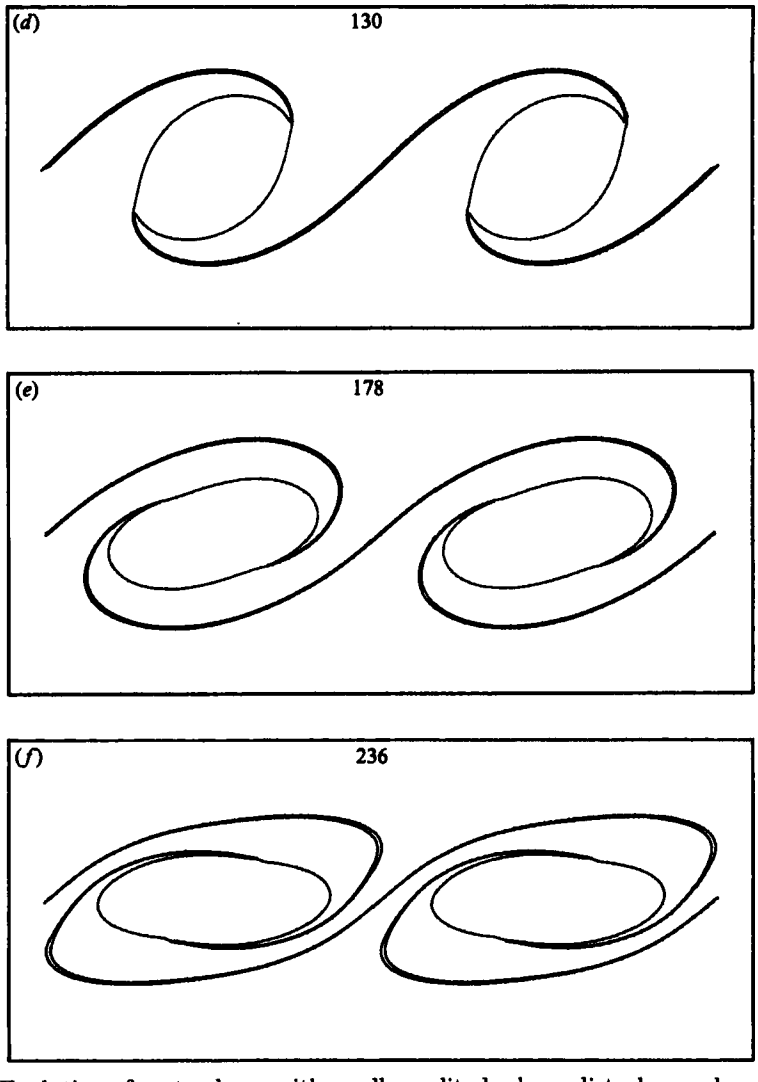

FIGURE 5. Evolution of vortex layer with small-amplitude shape disturbance; layer thickness, $kb = 1.00$. (*a*) $t' = 0$; (*b*) 12.0; (*c*) 21.0; (*d*) 25.5; (*e*) 28.8; (*f*) 31.6.

section, but the profiles will be identical after the decaying normal modes have disappeared.

We wish to examine the effect of a small, but not infinitesimal, disturbance on a thin vortex layer. We choose $\alpha_0 k = 0.03$ on a layer of thickness $kb = 0.125$. Although $\alpha_0 k$ is extremely small, the value of α_0/b is approximately 0.25; linear theory assumes both quantities to be negligible. Figure 7 (*a*) shows the form of the initial disturbance. As is easily seen, the circulation per unit length is significantly perturbed even for this small amplitude. Comparing with figure 2 (*a*), we might infer that a circulation disturbance constitutes a stronger perturbation on thin layers. Because it starts with an initial accumulation of vorticity, the circulation disturbance grows more rapidly than the shape disturbance, with greater overall accumulation at an earlier stage. At any given instant, the circulation disturbance has a greater amplitude than the shape disturbance with the same initial amplitude.

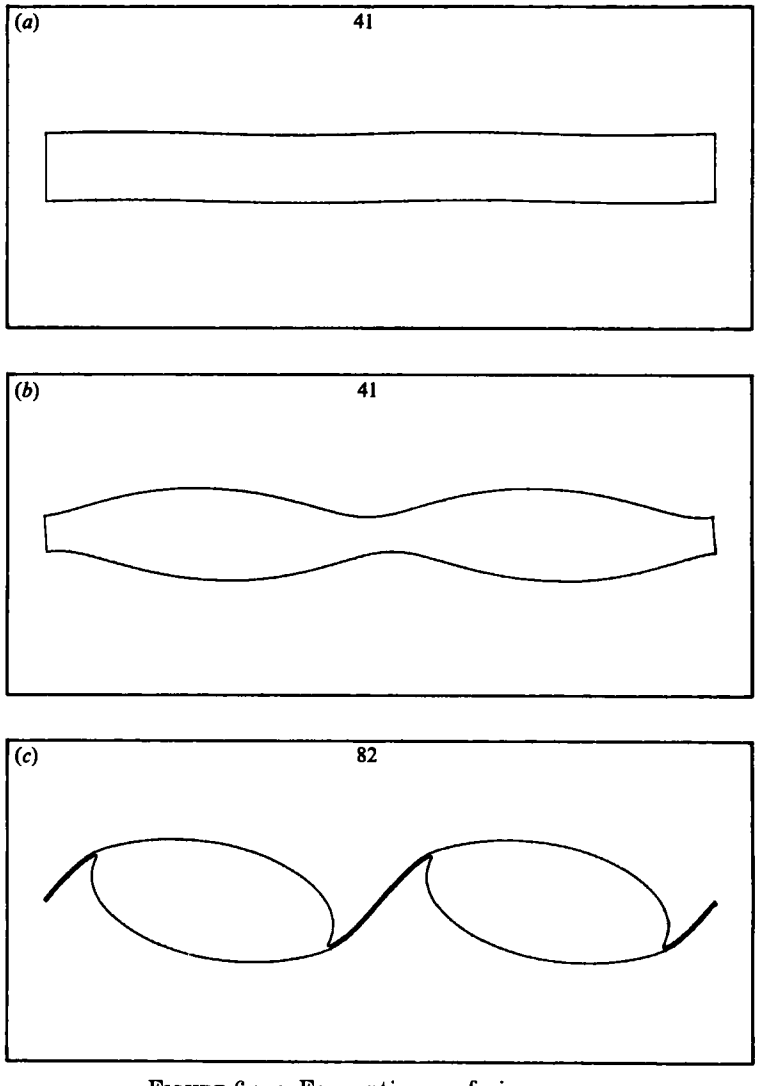

FIGURE 6 *a–c*. For caption see facing page.

Similar calculations have been performed on thicker layers with the same initial amplitude $\alpha_0 k = 0.03$. The same qualitative behaviour is observed, but the differences with the shape disturbances diminish as the thickness increases. This is to be expected, since the ratio α_0/b decreases when the thickness kb is increased for constant $\alpha_0 k$. Thus, for a thick layer, $kb = 1.00$, the development of a circulation disturbance is nearly indistinguishable from that of the shape disturbance previously shown in figure 5.

3.4. *Shape disturbances – finite amplitude*

In the calculations presented above, we considered disturbances with small initial amplitude. For the most part, the early stages in the growth of these layers is predicted by linear theory. At this point, we would like to analyse the evolution of layers subject to finite disturbances. In real flows, the perturbations may be of finite size and cannot be modelled by linear theory, even in the early stages. One of the

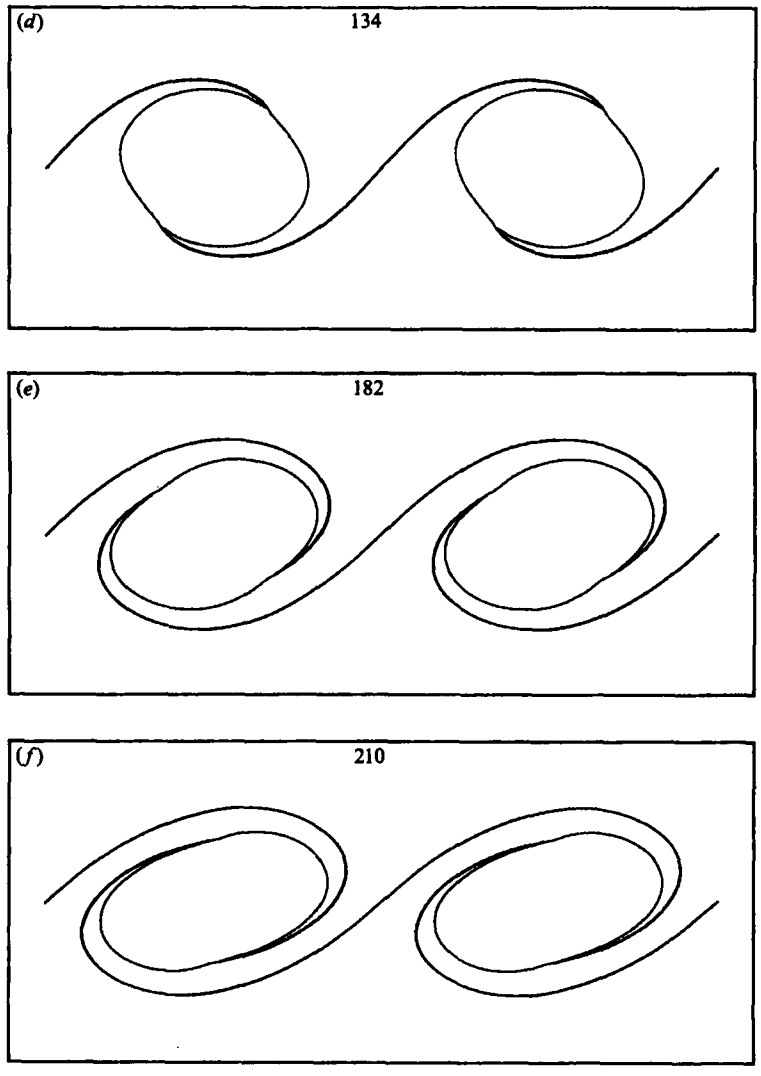

FIGURE 6. Evolution of vortex layer with small-amplitude shape disturbance; layer thickness, $kb = 1.278^{+}$, corresponds to neutral-stability point from linear theory. (*a*) $t' = 0$; (*b*) 26.0; (*c*) 35.0; (*d*) 39.0; (*e*) 42.5; (*f*) 43.9.

problems in studying finite-amplitude disturbances is in choosing the form of the initial disturbance. For infinitesimal amplitude, the choice of sinusoidal waves is quite general, because more general disturbances may be analysed through a Fourier decomposition. For large-amplitude disturbances with nonlinear interactions, this simplification does not apply, and the choice of initial disturbance involves some arbitrariness. We choose an initial perturbation in the form of finite-amplitude sine waves with the upper and lower boundaries specified in the manner described above. While this is an arbitrary choice, it is the most natural one and will provide a closer comparison with the small-amplitude cases studied above.

In the examples which follow, we shall restrict our attention to shape disturbances, $\phi = 0$, and consider layers of different thicknesses, each with initial amplitude $\alpha_0 k = 0.50$. Figure 8 shows the evolution of a disturbance for the thinnest layer,

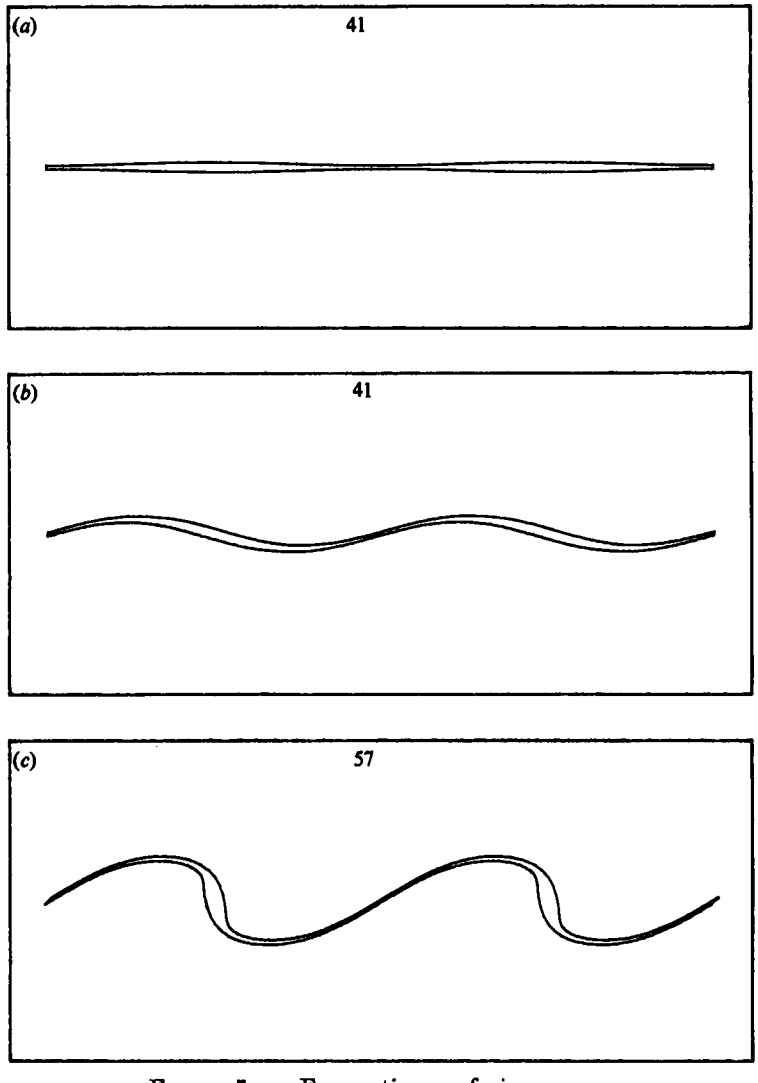

FIGURE 7 *a–c*. For caption see facing page.

$kb = 0.125$. The first view, figure 8 (*a*), shows the magnitude of the initial perturbation, while the next frame, figure 8 (*b*), shows the early accumulation of vorticity along the layer. Although this development appears qualitatively similar to that observed for small disturbances, we notice a slight difference in the thinning near the midpoint of the core region. This is more easily observed in the succeeding view, figure 8 (*c*), where the central region has split into two well-defined vortex cores. At later times, figure 8 (*d–f*), the 'braid' connecting the two cores becomes extremely thin, while the two vortex regions form compact cores which orbit each other in a quasi-steady motion. The position of the cores is quite stable, and figure 8 (*f*) may be viewed as the asymptotic state for this layer.

The bifurcation into two vortex cores is the most dramatic difference between the large- and small-amplitude disturbances. A second feature which is not as readily apparent is that the cores contain more vorticity and the wings are much thinner for the large-amplitude disturbance. The cores contain nearly 50% of the total

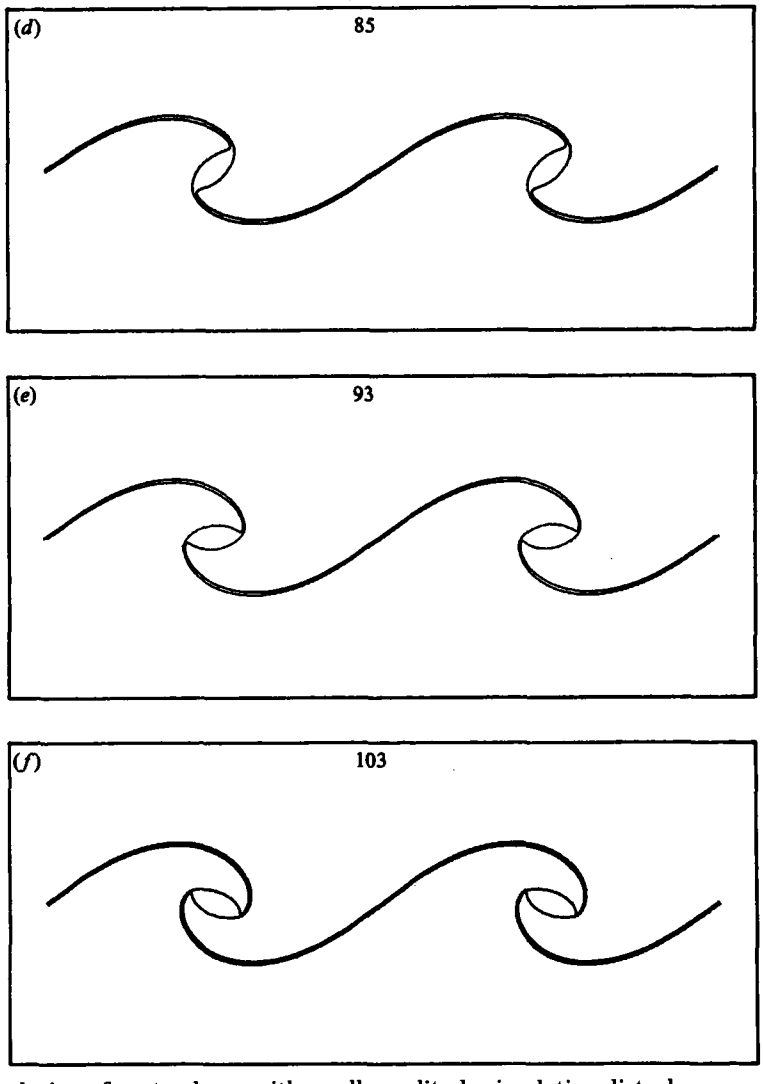

FIGURE 7. Evolution of vortex layer with small-amplitude circulation disturbance, $\alpha_0 k = 0.03$; layer thickness, $kb = 0.125$. (*a*) $t' = 0$; (*b*) 11.0; (*c*) 25.0; (*d*) 31.0; (*e*) 34.0; (*f*) 36.4.

vorticity in this case, as compared with 25 % previously. Thus, each of the vortex cores in figure 8 contains approximately the same vorticity as the core shown in figure 2.

Proceeding to layers of greater thickness, in figure 9 we examine the layer with $kb = 0.175$. For small amplitudes, this layer showed behaviour essentially identical with that of the $kb = 0.125$ layer. In the present case, the behaviour is similar in the early stages, figure 9(*a*,*b*), but the thicker layer does not show the indentation in the emerging core. At later times, the development is quite different with the formation of a single elongated S-shaped core. There appears to be a critical thickness below which the vortex region splits into two cores. We conclude that this critical thickness depends on the initial amplitude (and form) of the disturbance, since we observed the formation of a single core for all small disturbances. If the critical thickness is a function of initial amplitude, then a larger disturbance might produce bifurcation for the $kb = 0.175$ layer. We considered an initial amplitude of $\alpha_0 k = 1.0$ and found

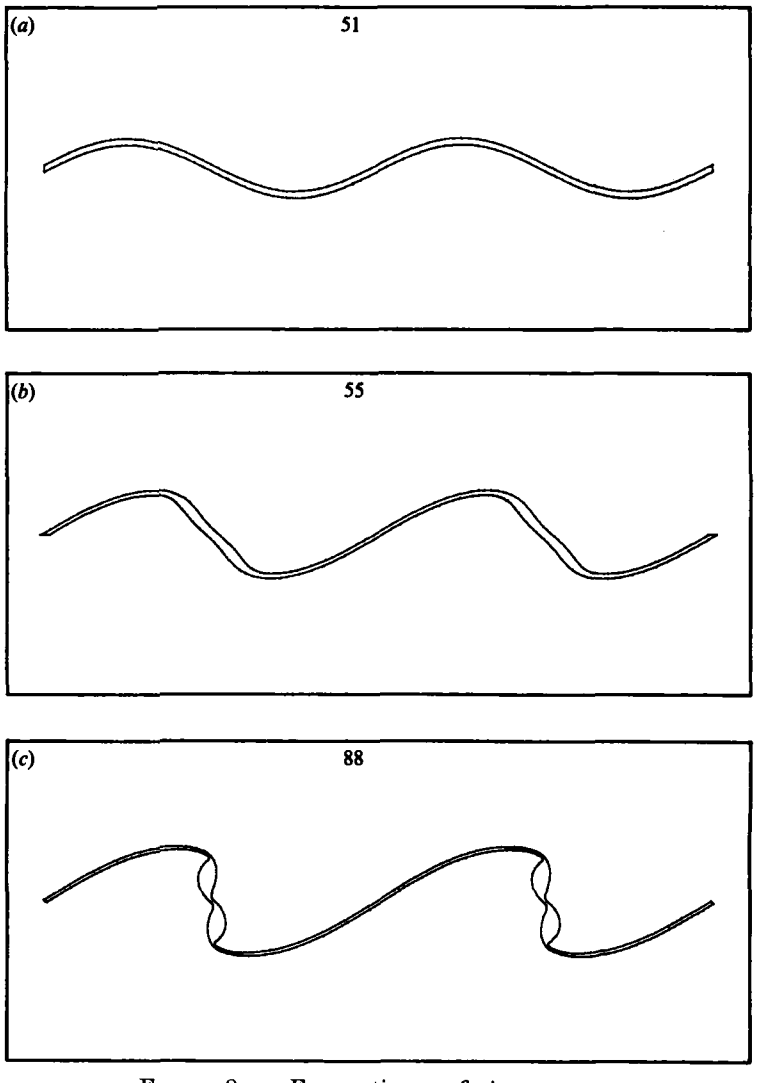

FIGURE 8 *a–c*. For caption see facing page.

that two cores developed. Thus for a layer of thickness $kb = 0.175$, we have found three different types of motion: compact elliptical cores for small amplitudes, elongated S-shaped cores for intermediate amplitudes and bifurcation into two cores for large amplitudes. Taken together with the results for the $kb = 0.125$ layer, we infer that this behaviour is not unique, but is characteristic of finite disturbances on all thin vortex layers.

We continue our investigation by considering a finite-amplitude disturbance on a $kb = 0.50$ layer. Comparing the results for this layer, figure 10, with the earlier results for small disturbances, figure 4, we see that the evolution is almost identical in the later stages. The only significant difference is in the time required for roll-up, with a shorter time in figure 10 owing to the larger initial amplitude. The development of a finite disturbance on a layer of thickness $kb = 1.00$ is shown in figure 11. Based on our experience with the $kb = 0.50$ layer, we might not expect any significant change from the small-amplitude case. This expectation proves incorrect, as can be seen from

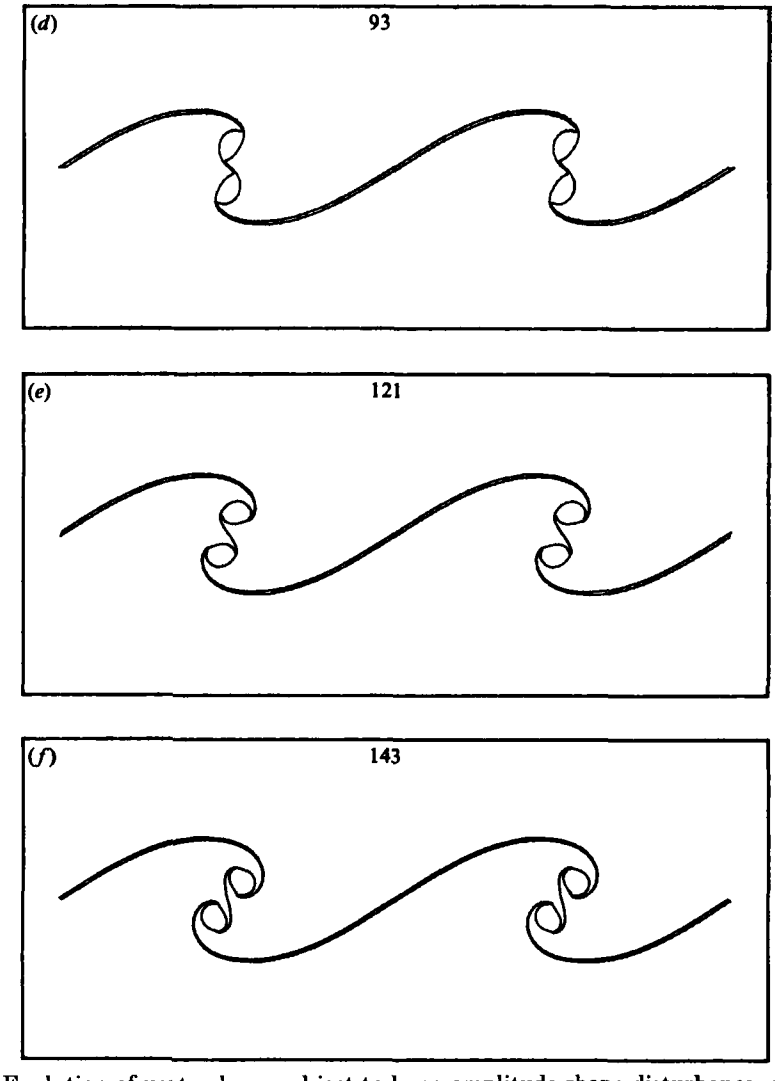

FIGURE 8. Evolution of vortex layer subject to large-amplitude shape disturbance, $\alpha_0 k = 0.50$; layer thickness, $kb = 0.125$. (*a*) $t' = 0$; (*b*) 19.8; (*c*) 29.0; (*d*) 30.5; (*e*) 33.8; (*f*) 36.8.

a comparison of figures 5 and 11. In the intermediate stages, figures 5(*c*,*d*); 11(*c*,*d*), the motions appear qualitatively similar, but the later stages, figures 5(*e*,*f*); 11(*e*,*f*), show marked differences. The large-amplitude disturbance has developed a smaller less elongated core with more vorticity in the wings. Reversing the earlier trend, we find 30 % of the vorticity in the wings as opposed to only 10 % for the small-amplitude motion. Another noteworthy feature is that the vortex cores in the present case do not rotate, but form stationary regions of vorticity around which the wings circulate. The attachment points of the wings precess around the perimeter, and the fluid within the core rotates, but the axis of the elliptical core remains horizontal. As time progresses, the cores remain stationary, but the vorticity in the outer part of the wings is convected downstream into adjacent cells.

The motion of a $kb = 1.278^{+}$ layer is similar to that of the $kb = 1.00$ layer, and we do not show the full evolution. Instead, we present the final state for a number of

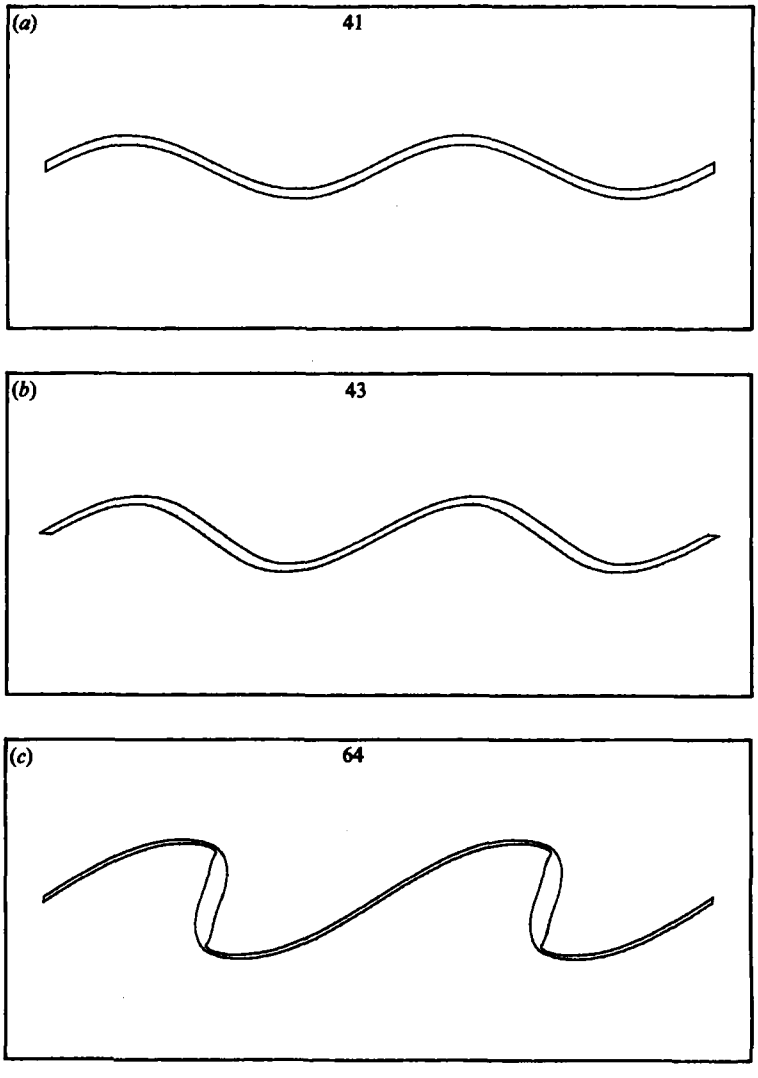

FIGURE 9 *a–c*. For caption see facing page.

different layers to summarize the effect of layer thickness on the development of large-amplitude disturbances. Each of the layers shown in figure 12 was perturbed with a sinusoidal-shape disturbance with $\alpha_0 k = 0.50$. We identify three distinct types of behaviour. For the thinnest layers, $kb = 0.100$ and 0.125, two vortex cores form in a stable orbiting configuration. As a critical thickness is reached, $kb = 0.150$, a single vortex forms, which progresses from an S shape, $kb = 0.175$, to a more rounded elliptical shape, $kb = 0.50$. This single core rotates at nearly constant angular velocity whose magnitude decreases as the thickness of the layer is increased. For the thickest layers, $kb = 0.80$–1.50, the single large vortex core remains stationary while the wings circulate around the core. In the later stages of these motions, significant amounts of vorticity in the wings are convected into adjoining periods along the layer.

The profiles shown in figure 12 cover a wide range of layer thicknesses, but it is not clear whether they represent the full range of behaviour. The $kb = 1.50$ layer

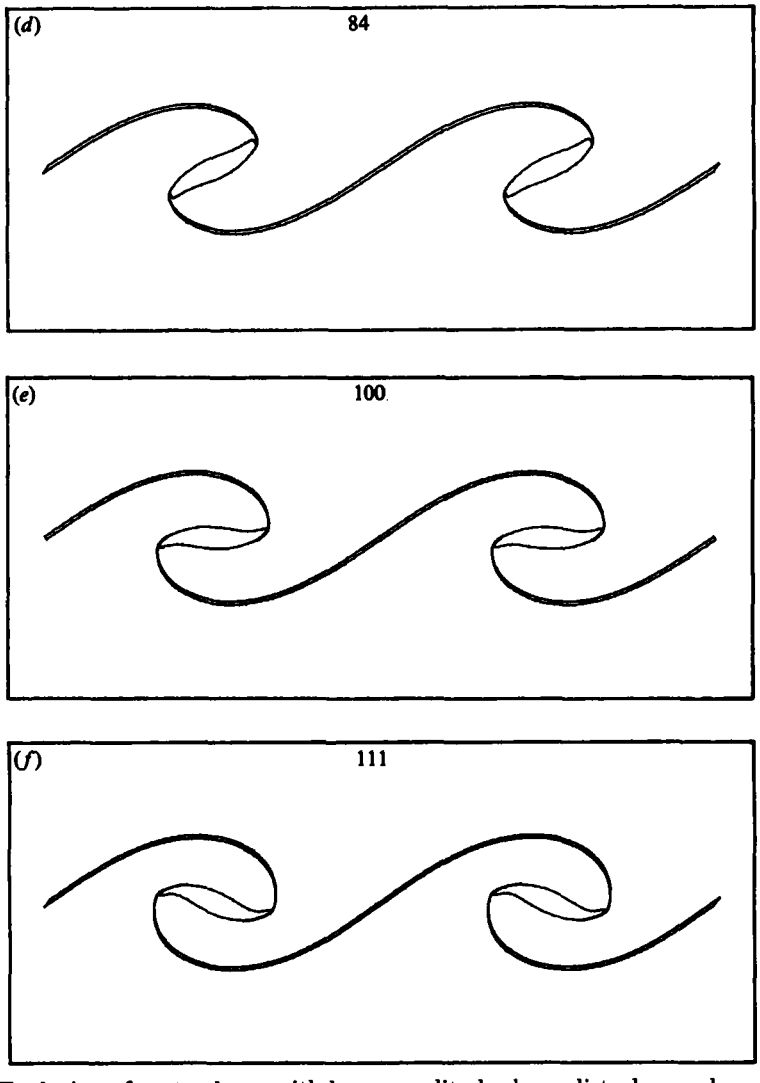

FIGURE 9. Evolution of vortex layer with large-amplitude shape disturbance; layer thickness, $kb = 0.175$. (*a*) $t' = 0$; (*b*) 9.9; (*c*) 23.2; (*d*) 28.6; (*e*) 32.0; (*f*) 34.8.

seems to be a good approximation to the thickest layers, since larger values are stable to small disturbances, and the final stage pictured in figure 12 shows only marginal increase over the initial amplitude of the disturbance. At the other end of the scale, we might question whether $kb = 0.100$ represents the limiting behaviour for thin layers. In particular, we consider whether infinitesimal values of $\alpha_0 k$ would lead to double vortex cores on infinitesimally thin layers. To answer this question, we considered shape disturbances on zero-thickness vortex sheets using the method described by Higdon & Pozrikidis (1985). For small-amplitude disturbances with $\alpha_0 k = 0.03$, we found a single vortex core, while, for disturbances larger than $\alpha_0 k = 0.10$, two vortex cores appeared. In each case, the vortex core is in the form of an exponential spiral with singular circulation at the centre. We conclude that, for disturbances below a certain finite amplitude, a single core forms independent of the thickness of the layer. Thus, we expect that $kb = 0.100$ is a reasonable representation of the asymptotic behaviour for finite-thickness vortex layers.

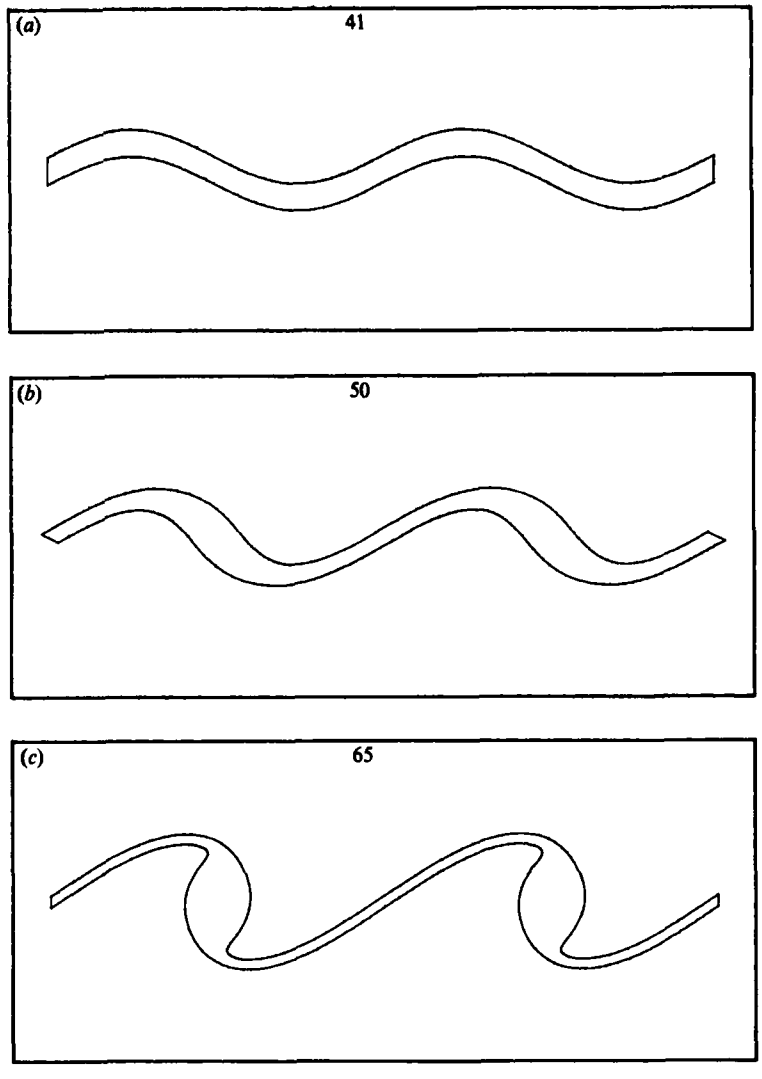

FIGURE 10 *a–c*. For caption see facing page.

Considering the range of behaviour we have observed for large-amplitude disturbances, it is of interest to review past efforts which have shown similar behaviour. First, with respect to the stationary vortex cores in figure 12(*f–i*), we note that Pierrehumbert & Widnall (1981) discovered a class of steady-state solutions for periodic regions of constant vorticity with nearly elliptic shape. Saffman & Szeto (1981) arrived at the same class of solutions by an independent method. For steady state, these solutions require a specific relationship between the eccentricity and the vortex spacing. The spacing and eccentricity of the steady cores in figure 12 are in excellent agreement with these results.

The bifurcation of the vortex cores for large disturbances on thin vortex layers may be anticipated from a number of previous results. Birkhoff (1962) found similar behaviour for large disturbances on vortex sheets using a simple point-vortex model. Love (1894) showed that an elliptical-vortex region has a critical eccentricity, $e = 3.0$, above which the vortex is unstable to small disturbances. Thus, it is not surprising

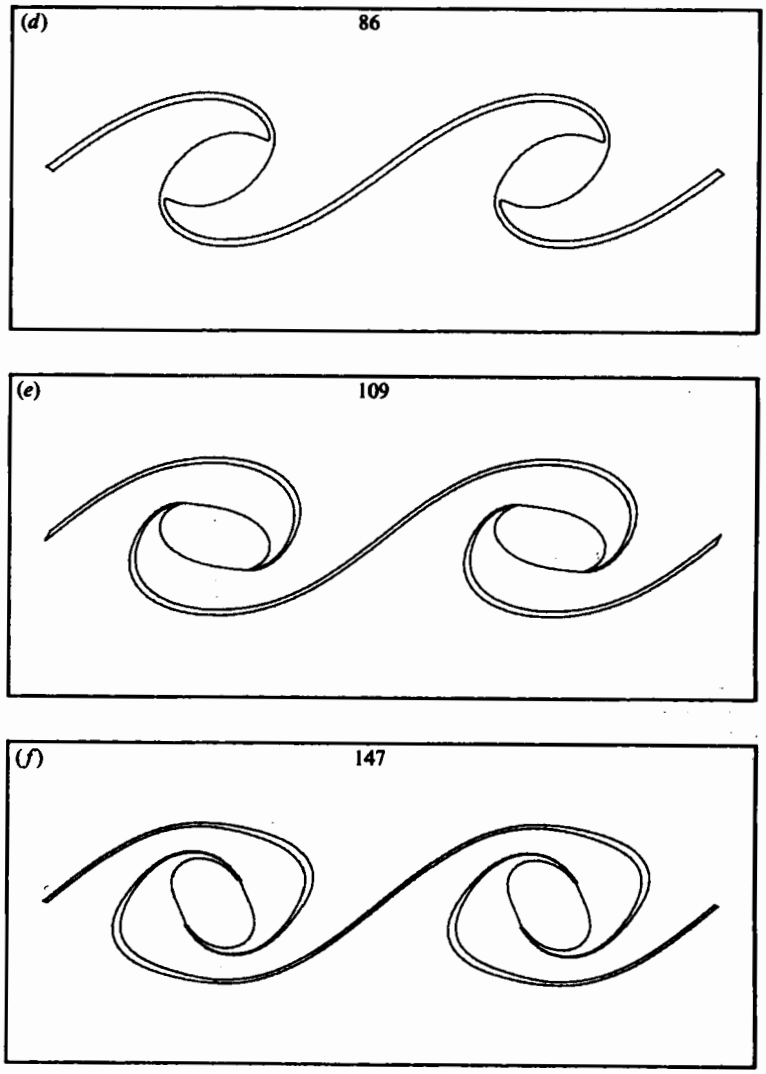

FIGURE 10. Evolution of vortex layer with large-amplitude shape disturbance; layer thickness, $kb = 0.50$. (*a*) $t' = 0$; (*b*) 5.6; (*c*) 10.4; (*d*) 14.1; (*e*) 18.4; (*f*) 21.6.

that we see bifurcation of narrow vortex cores. For comparison, the eccentricity of the elliptical core in figure 12(*c*) is approximately $e = 4.5$. Approaching the question of stability from the other side, Saffman & Szeto (1980) demonstrated the existence of steady-state solutions with rotating cores. Overman & Zabusky (1982) considered the stability of such solutions and showed that there is a critical separation distance below which the cores will coalesce. This coalescence leads to the formation of S-shaped cores similar to those appearing in figure 12(*d*).

A final point to consider is the effect of finite amplitude on circulation disturbances. In this case, the amplitude is limited by the constraint that it must be less than half the layer thickness to avoid overlap of the upper and lower boundaries. Within the limits dictated by this constraint, we found no qualitative difference between small- and large-amplitude circulation disturbances. In all cases, a single rotating core was formed. Similarly, circulation disturbances on vortex sheets always lead to a single core.

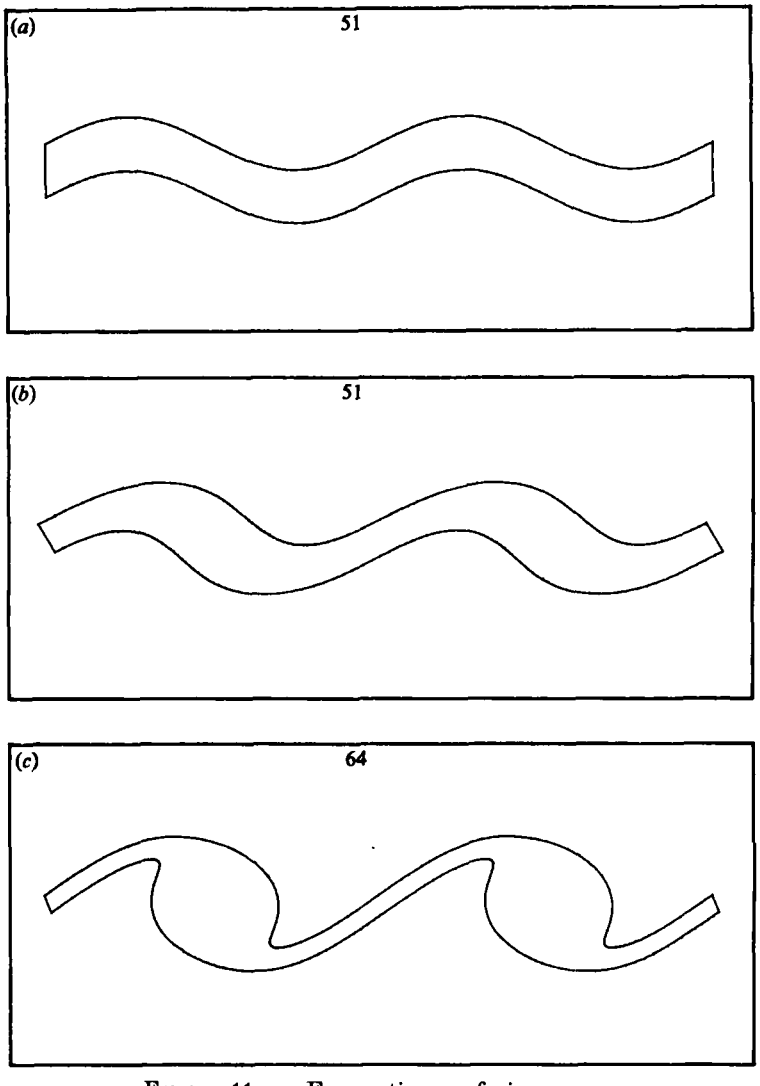

FIGURE 11 *a–c*. For caption see facing page.

3.5. *Streamline patterns*

We have examined detailed figures showing the evolution of vortex layers and their dependence on the disturbance parameters. At this point, we find it instructive to examine the fluid velocity field by showing the instantaneous streamlines for three layers at a late stage in their development. Figure 13 shows the streamlines for layers with initial thickness $kb = 1.00$, 0.50 and 0.125, all subject to large-amplitude disturbances $\alpha_0 k = 0.50$. For the thickest layer, figure 13 (*a*), the streamlines are nearly tangential to the contour of the vortex core-indicating that this contour is essentially stationary. The streamlines near the wings are horizontal, which shows that the fluid is being convected downstream carrying the vorticity into adjacent periods along the layer. In the intermediate-thickness layer, figure 13 (*b*), the streamlines intersect the vortex core at an appreciable angle showing the rotation of the core. In this case, the velocity in the vicinity of the wings is dominated by the rotating core; hence

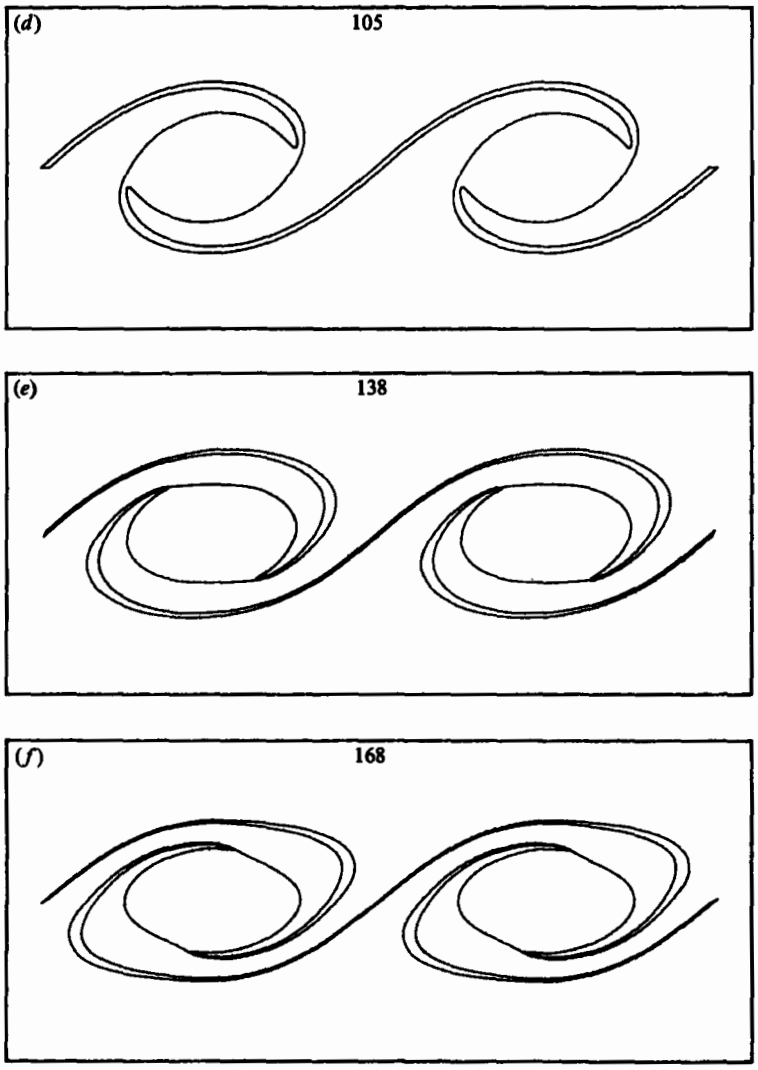

FIGURE 11. Evolution of vortex layer with large-amplitude shape disturbance; layer thickness, $kb = 1.00$. (*a*) $t' = 0$; (*b*) 2.5; (*c*) 6.0; (*d*) 11.5; (*e*) 15; (*f*) 16.5.

these regions circulate around the core and are not drawn downstream. The streamlines for the thinnest layer, figure 13(*c*), are similar to the preceding case in the outer regions of the layer, but differ significantly near the core. Here there is a separate region of rotating fluid in each of the cores with a separating streamline encircling the two regions. These three streamline patterns are characteristic of the types of motion we have observed on finite vortex layers.

4. Growth rate of disturbances

In the foregoing discussion, we have examined the profiles which develop when a shear layer is subjected to periodic disturbances but have made only qualitative reference to the rate at which these motions proceed. In the present section, we wish to provide a detailed analysis of the growth rates indicating how they are affected

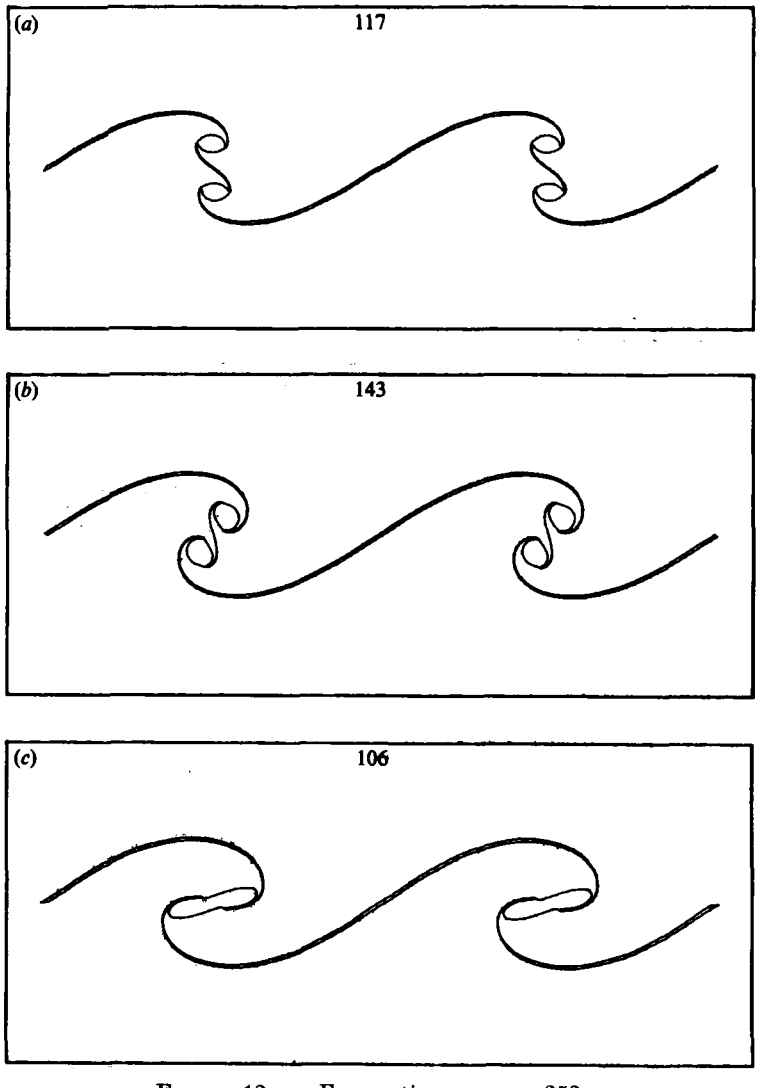

FIGURE 12 *a–c*. For caption see page 252.

by the disturbance parameters. Before proceeding with a discussion of the growth rate, we need to clarify the method by which the variables are to be non-dimensionalized. As noted previously, the layer is characterized by the wavenumber k, the initial amplitude α_0, the thickness b and the vorticity ω. We define the amplitude α to be the maximum displacement, at successive times, from the undisturbed position and use the non-dimensional form α/α_0. This provides a natural comparison with linear theory. With respect to the non-dimensionalization of time, there are two obvious choices each of which is meaningful in a specific physical context. The first choice is $t' = \omega t$, which considers the vorticity to be the reference scale. This non-dimensionalization is appropriate for studying the response of a layer of given thickness to disturbances of varying wavelength. The second choice for time is to define $t'' = kb\omega t$. This choice is the most natural when studying the effect of layer thickness. Thus we consider not constant vorticity, but constant total shear across the layer. Such a situation arises when a layer is forced at constant wavelength, but

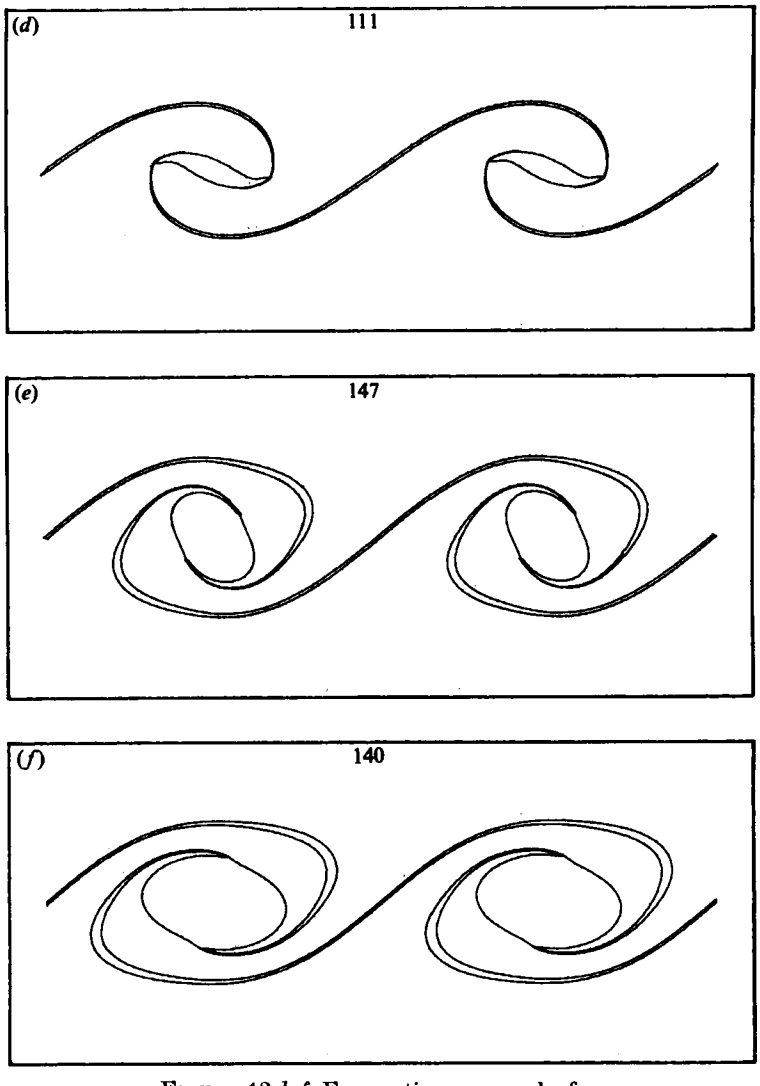

FIGURE 12 *d–f*. For caption see overleaf.

its thickness changes slowly owing to diffusion of vorticity. In the limit of small thickness, the layer behaves as a vortex sheet. As we shall see, these two choices lead to markedly different interpretations of the growth rate.

4.1. *Linear theory*

We shall start our discussion by reviewing certain important results from linear theory. As is usual, we find that the linearized model predicts exponential growth of the form $\alpha = \alpha_0 e^{ct}$ or in non-dimensional form $\alpha/\alpha_0 = e^{c't'}$. Even in linear theory, the non-dimensionalization of t leads to different interpretations. Figure 14 shows the growth rate as a function of kb according to linear theory. The dashed line shows the classical result for c' with short waves, $kb > 1.278$, stable and a maximum growth rate for $kb = 0.80$. The solid line shows the growth rate c'' corresponding to $t'' = kb\omega t$. Considering the wavelength to be constant, we now infer that thick layers are stable, while the growth rate approaches its maximum value for asymptotically thin layers. This is simply the growth rate predicted by linear theory for vortex sheets.

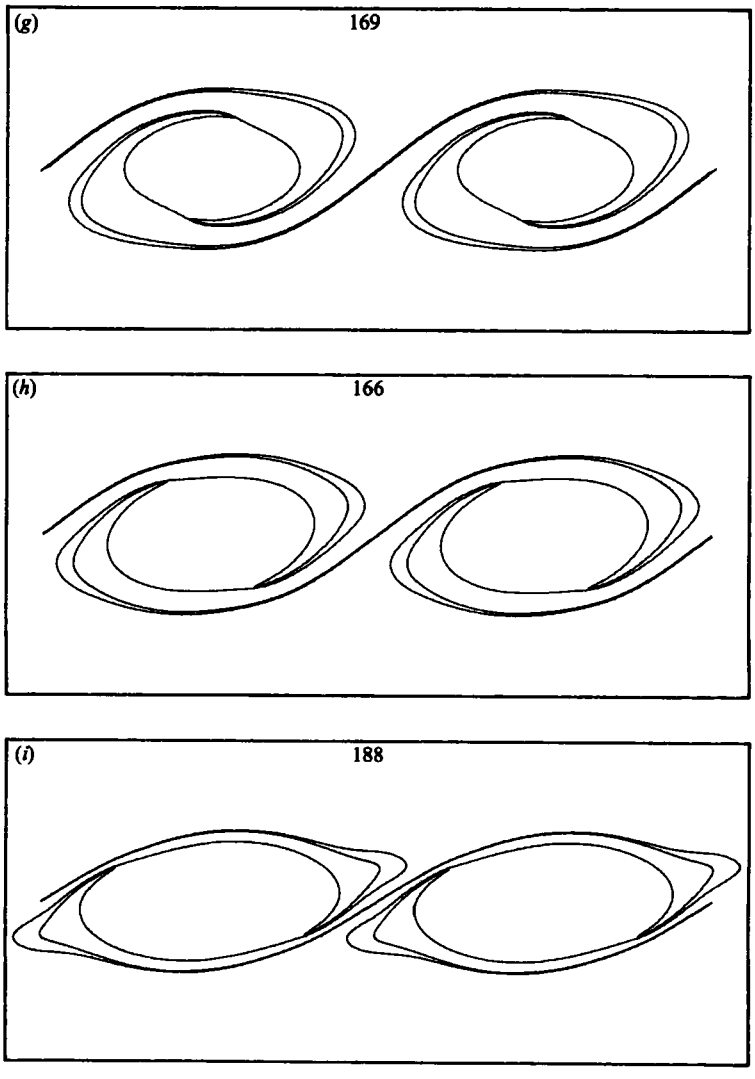

FIGURE 12. Final states for vortex layers of varying thickness subject to large-amplitude shape disturbances. (*a*) $kb = 0.100$; (*b*) 0.125; (*c*) 0.150; (*d*) 0.175; (*e*) 0.500; (*f*) 0.800; (*g*) 1.000; (*h*) 1.278; (*i*) 1.500.

One additional feature of the motion which may be examined through the use of linear theory is the effect of the phase ϕ on the initial growth rate. For unstable disturbances, an arbitrary phase ϕ may be split into two component phases, representing the growing and decaying normal modes. For large time, the decaying mode dies away, and all phases grow at the same rate corresponding to the growing normal mode. It is important to realize, however, that the initial growth rate, and hence the amplitude at any later instant will depend on the initial phase. Figure 15 shows the amplitude as a function of time for four different phases on a layer of thickness $kb = 0.125$. The dashed lines are from linear theory, while the solid lines are from our numerical calculations. The curve labelled ϕ_{nm} is a straight line, because its phase is exactly that of the growing normal mode. Note that the other phases show both greater and smaller initial growth rates. The curve $\phi = 0$ represents shape

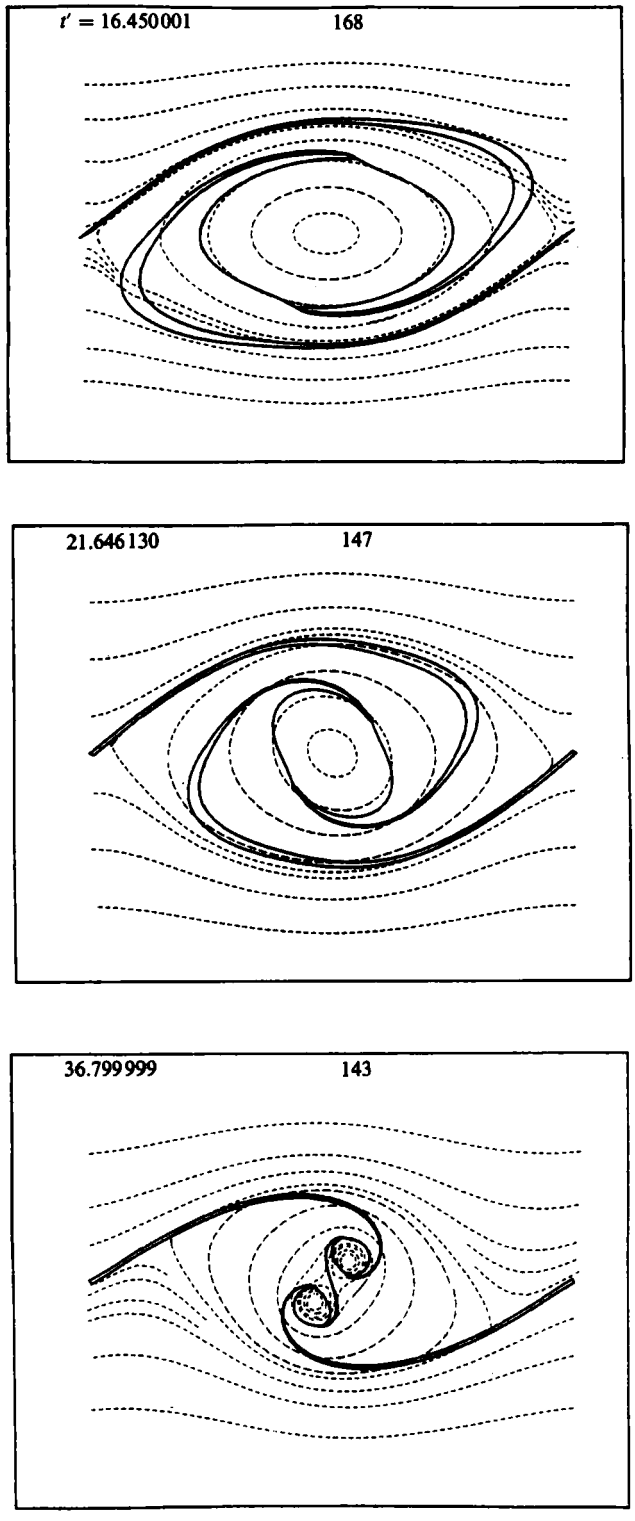

FIGURE 13. Instantaneous streamline patterns for layers of three different thicknesses showing characteristic development of a vortex layer.

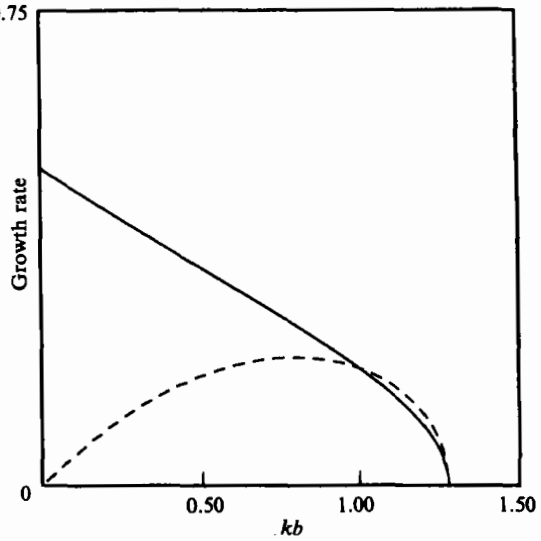

FIGURE 14. Growth rate predicted by linear theory as a function of thickness kb. Dashed line gives result for c' defined with respect to dimensionless time $t' = \omega t$. Solid line gives result for c'' defined with respect to dimensionless time $t'' = kb\omega t$.

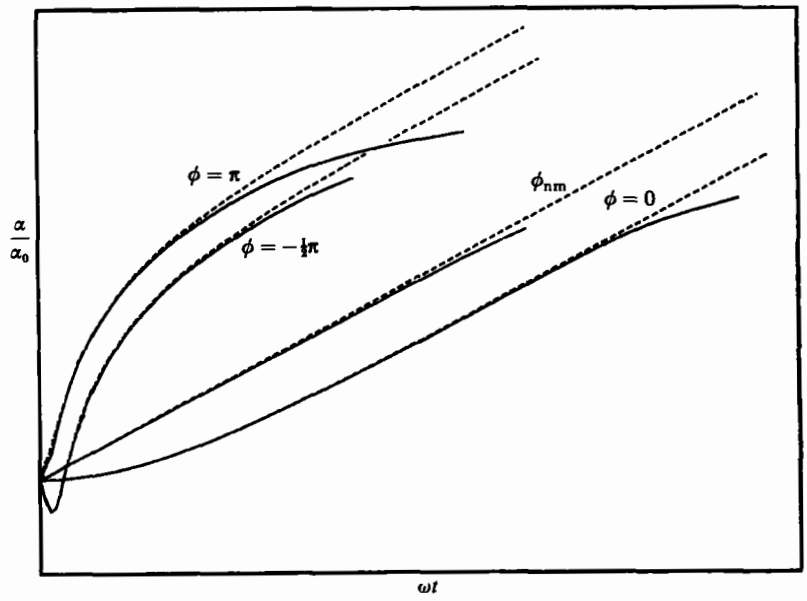

FIGURE 15. Amplitude of disturbance *versus* time plotted on logarithmic axis. Dashed lines show linear theory, solids lines results of numerical calculations. Different curves correspond to different values of the phase difference ϕ between upper and lower boundary perturbations. Curve labelled ϕ_{nm} represents growing normal mode.

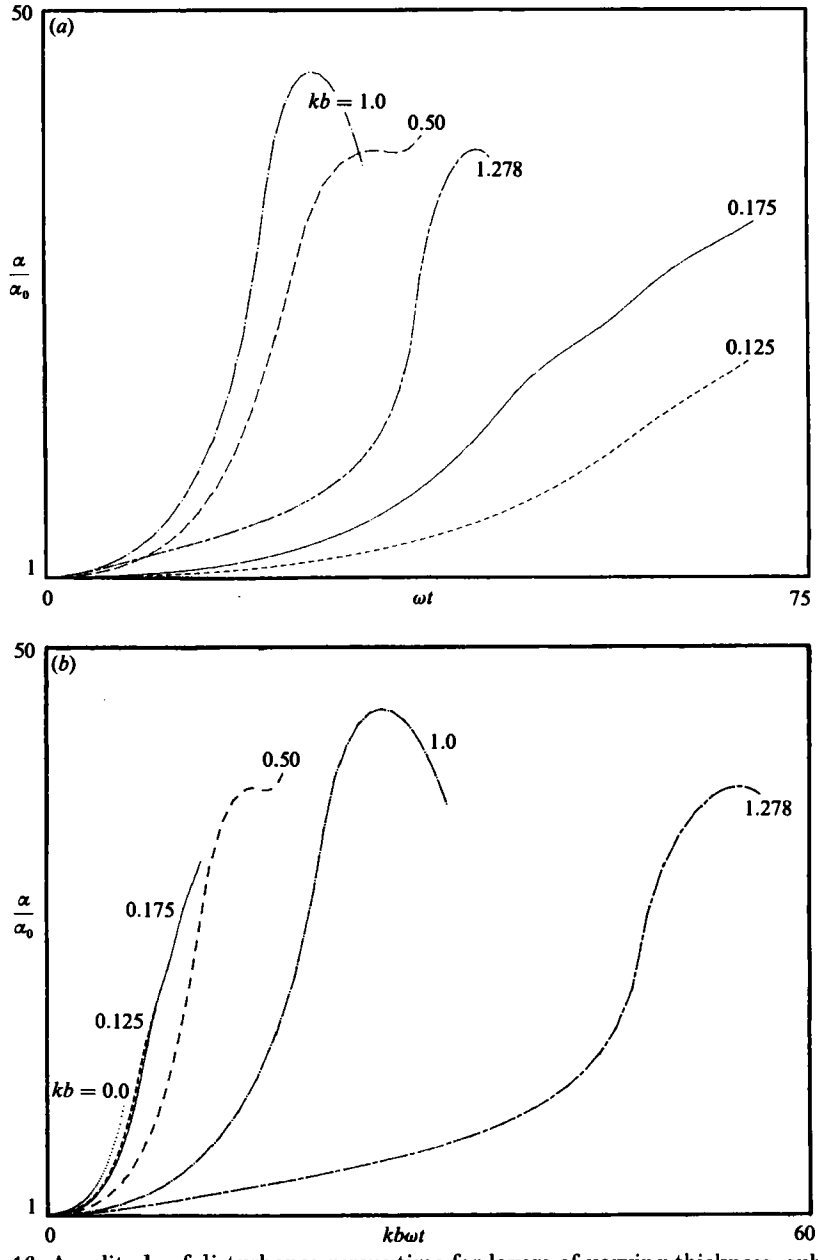

FIGURE 16. Amplitude of disturbance *versus* time for layers of varying thickness, subject to small-amplitude shape disturbances. Abscissa: (*a*) $t' = \omega t$; (*b*) $t'' = kb\omega t$.

disturbances, while $\phi = \pi$ refers to circulation disturbances. Negative values of ϕ show an initial decay, because they have a large component corresponding to the decaying normal mode.

4.2. *Growth rates for nonlinear disturbances*

The results from linear theory discussed above provide an accurate picture of the initial evolution of the vortex layers. For later times, the nonlinear interactions lead to a decrease in the growth rate and finally to a bounded amplitude. Figure 16 shows

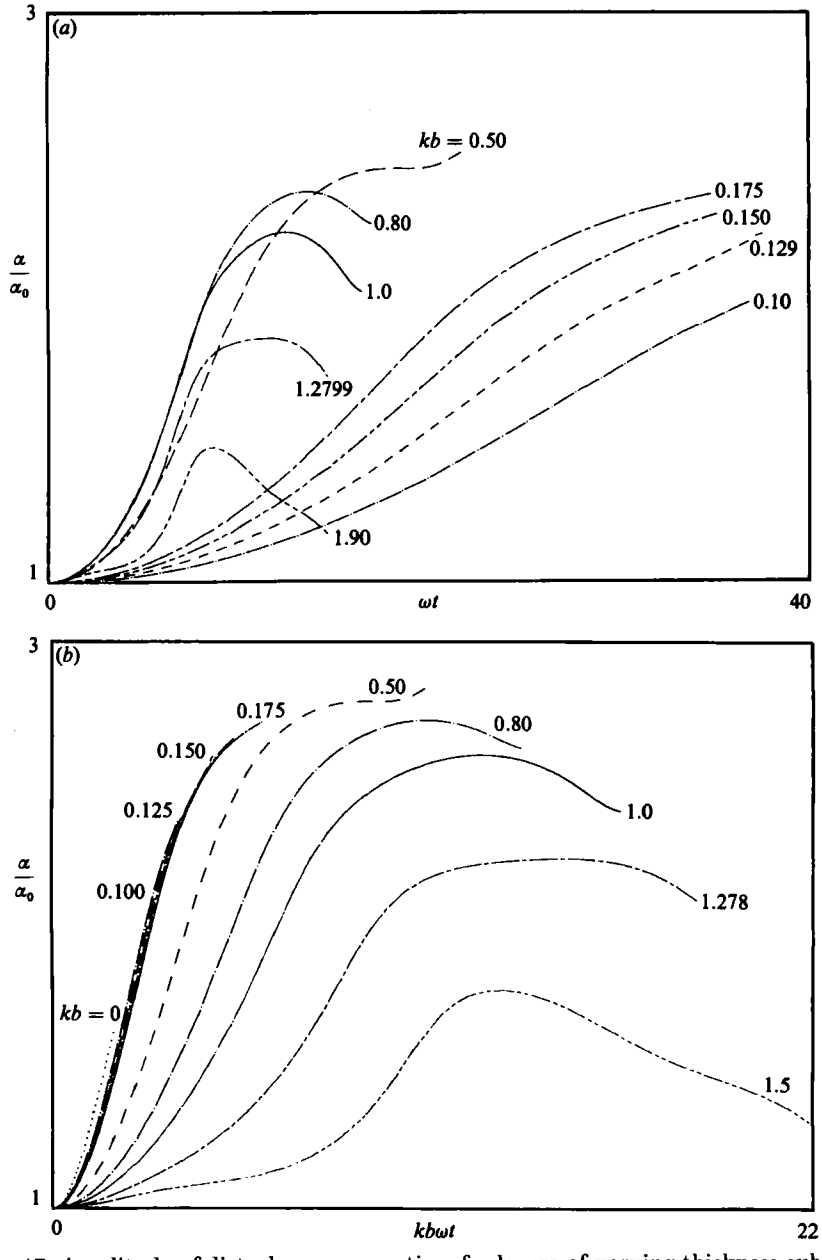

FIGURE 17. Amplitude of disturbance *versus* time for layers of varying thickness subject to large-amplitude shape disturbances. Abscissa: (*a*) $t' = \omega t$; (*b*) $t'' = kb\omega t$.

the growth of disturbances for several different layers with initial amplitude $\alpha_0 k = 0.03$ as a function of time. The curves are plotted *versus* t' and t'' in figure 16(*a*, *b*). In the first figure, we see the expected result that the $kb = 0.50$ and $kb = 1.00$ layers grow most rapidly, since these are near the maximum growth rate from linear theory. It is interesting to note that the $kb = 1.278$ layer grows faster than the others, but at a linear rate, as opposed to the exponential rate of the unstable layers. The thinner layers, $kb = 0.125$ and $kb = 0.175$, grow more slowly simply because there is less vorticity, and the velocities are correspondingly smaller. These

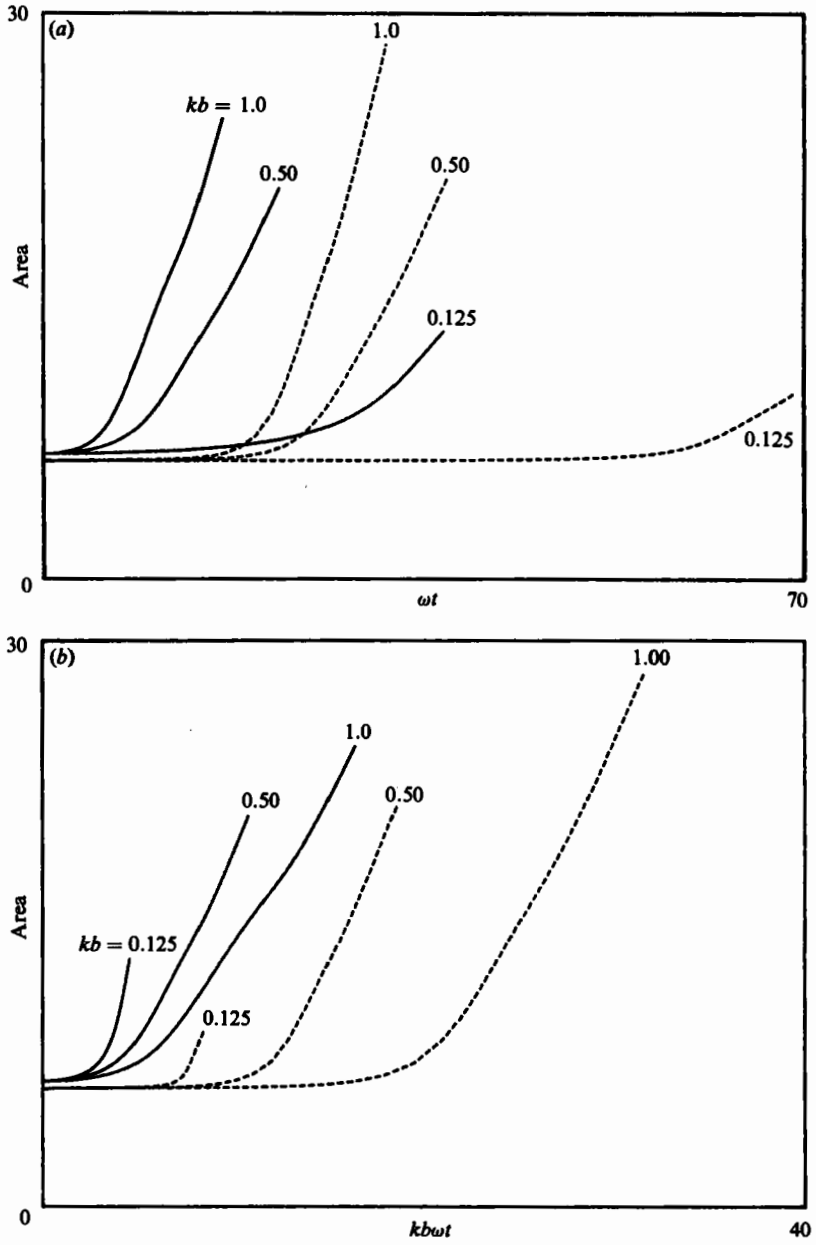

FIGURE 18. Interfacial area as a function of time for layers of varying thickness. Dashed lines are small-amplitude shape disturbances; solid lines are large amplitude. Abscissa: (*a*) $t' = \omega t$; (*b*) $t'' = kb\omega t$.

layers will eventually reach an amplitude of the same order as the other layers. It is interesting to note the appearance of a maximum and subsequent decrease in the amplitude of the thicker layers. This is not due to a decay, but rather to an oscillation caused by the rotation of the elliptical vortex core. The peak in amplitude occurs when the major axis of the core is vertical. The elliptical core for the $kb = 0.50$ layer rotates more rapidly, and we see the amplitude begin to rise after going through a local minimum.

A different view of the growth is shown in figure 16(*b*), where the amplitude is plotted *versus* t''. Here we find that the thinnest layers grow most rapidly with a monotonic decrease in the growth rate for decreasing thickness. This is consistent with linear theory and is easily explained by the fact that each layer represents the same total velocity shear. Thus it is natural that the more concentrated shear in the thinner layers should lead to a more rapid growth of disturbances. As indicated above, all layers will eventually reach comparable amplitudes. Thus we find that the final amplitude of the layer is of order 0.2 times the wavelength and is nearly independent of the initial thickness of the layer.

The results just presented were for small initial amplitudes; for finite initial amplitude $\alpha_0 k = 0.50$, the growth rates are shown in figure 17(*a*,*b*). The results in these figures are essentially similar to those for the small amplitudes; however, there are a few significant differences. First, we note that the thickest layers now show a somewhat smaller final amplitude, and the $kb = 1.50$ layer has decaying amplitude as might be expected. On the other hand, the $kb = 1.278$ layer more closely approaches the thinner layers. One of the interesting features of these growth curves revealed most clearly in figure 17(*b*) is that the bifurcation into two vortex cores does not seem to affect the growth rate. This is seen in the nearly identical curves for $kb = 0.100$–0.175. On the other hand, the formation of a steady non-rotating core for the large-amplitude disturbances on thick layers is apparent from the more gradual oscillation in the amplitude for the layers $kb = 1.00$ and 1.278. With the exception of the two stable layers, $kb = 1.278$ and 1.50, we find that the asymptotic amplitude is nearly constant for all layers and is again in the range 0.15–0.2 times the wavelength of the disturbance.

4.3. *Growth of interfacial area*

In the preceding discussion, we have examined the growth of disturbances through the maximum displacement of the boundaries. This is the most obvious measure of the growth rate, but there are other quantities of physical interest. One such quantity is the area of the interface between the mixing layers. This quantity is particularly important for chemical engineers studying reacting streams. If a reaction proceeds at a very fast rate and is thus diffusion limited, the rate of generation of products is directly proportional to the growth rate of interfacial area. Figure 18(*a*) shows the interfacial area as a function of t' for three different-thickness layers. In this figure, results are shown for both small, $\alpha_0 k = 0.03$, and large disturbances $\alpha_0 k = 0.50$. The most important conclusion to be drawn from these curves is that the growth rate approaches a constant value for each of the layers considered. This is consistent with the experimental results of Breidenthal (1981) who found a constant reaction rate as long as the mixing layer maintained a two-dimensional structure. Overall, the growth rates for interfacial area are consistent with the results for the growth rates of amplitude. Specifically, we note that the thinnest layer shows the smallest growth in area simply because the velocities are much smaller. The $kb = 1.00$ layer shows the fastest growth rate as before, and the large-amplitude disturbances develop more quickly than those of small amplitude.

A slightly different picture of the growth in area is given in figure 18(*b*), where the area is plotted *versus* t''. Here we see some interesting results arising from the timescaling. For small disturbances, all curves have essentially the same slope indicating identical growth rates. The only differences are in the time required to reach this asymptotic state. This implies that the different slopes observed in figure 18(*a*) may be attributed solely to the difference in the amount of vorticity in the

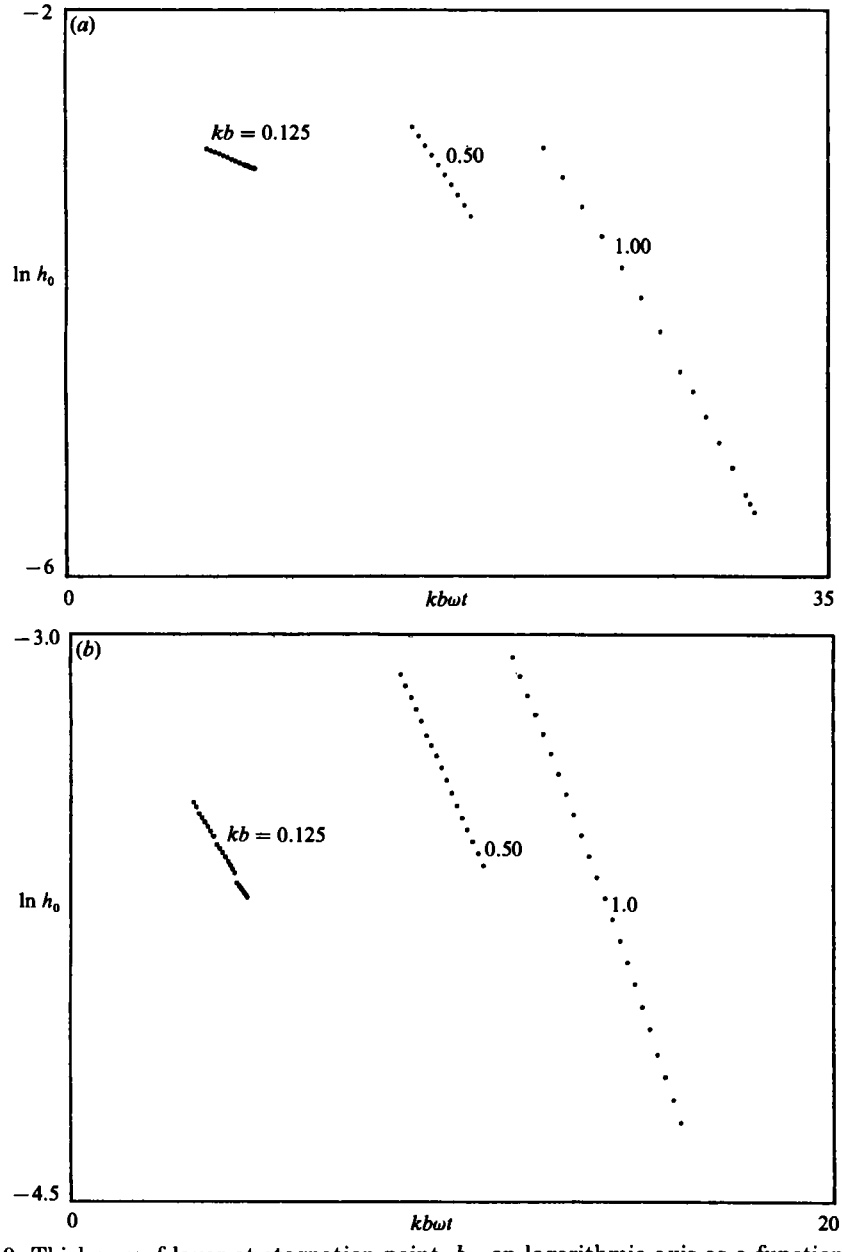

FIGURE 19. Thickness of layer at stagnation point, h_0, on logarithmic axis as a function of time for layers of different thickness. (*a*) Small-amplitude disturbance; (*b*) large-amplitude disturbance.

layers. Comparing the small-amplitude and large-amplitude curves in figure 18(*b*), we see a slight change in the growth rates. For large amplitudes, the $kb = 0.50$ layer has the same growth rate, while the $kb = 1.00$ rate is smaller and the $kb = 0.125$ rate is larger. These changes may be explained by examining the profiles of the layers in these cases. The large-amplitude disturbance on the $kb = 0.50$ layer was indistinguishable from its small-amplitude counterpart. The large-amplitude disturbance on the $kb = 0.125$ layer showed a bifurcation into two vortex cores, leading to more growth in interfacial area. Finally, the large-amplitude disturbance on the $kb = 1.00$

layer leads to a stationary vortex core which may be expected to lead to less rapid growth in area. Our general conclusion is that the initial disturbance and the resulting structure of the layer have a strong influence on the growth of interfacial area. Under all circumstances, the growth rate will approach a constant value after an initial start-up period.

4.4. *Thickness of vortex braids*

In all of the layers we have studied, we have noted the gradual thinning of the vortex wings or braids connecting the periodic vortex cores. As the evolution of a layer proceeds, these regions decrease monotonically in thickness. To analyse this phenomenon in more detail, we consider the rate at which this thinning occurs. A characteristic value h_0 is defined as the thickness at the midpoint of the braid, i.e. at the point where the layer crosses the symmetry plane. This is a stagnation point in the flow field. The thickness h_0 is plotted on logarithmic axes *versus* t'' for small disturbances, figure 19(*a*), and for large disturbances, figure 19(*b*). In both cases, the points fall along a straight line, indicating an exponential decrease in thickness. This simple decay law indicates a constant rate of stretching at the stagnation point; hence the extensional flow is induced primarily by the vortex cores and not by the vorticity in the braids themselves.

The information presented in figure 19 may be used in a qualitative discussion of the effect of a mild density difference across the vortex layer. In this case, there is baroclinic vorticity generation in the braids. A simple vorticity balance may be made to determine if the density difference is sufficient to maintain the level of vorticity in the braids or if the braids will continue to decay. In this balance, the rate of depletion is equal to $\mathrm{d}h_0/\mathrm{d}t$ from figure 19 and is independent of h_0. It does depend on the strength of the vortex cores and will increase as the total vorticity increases. A more detailed discussion of this mechanism is given by Corcos & Sherman (1976, 1984).

5. Discussion

We have seen a wide range of phenomena which may occur in nonlinear Kelvin–Helmholtz instability. At this point, it is appropriate to summarize our results and identify those features which are most important in relation to previous work and in interpreting real flows. Many investigators have shown patterns of vortex roll-up similar to those presented here. These studies have employed vortex methods such as the cloud-in-cell calculations of Aref & Siggia (1980) or have involved finite-difference solutions of the Navier–Stokes equations such as those discussed by Corcos & Sherman (1984). The most significant result of our calculations has been to show how differences in the initial conditions – thickness of the layer, initial amplitude and type of disturbance – affect the later development of the vortex layer. We have shown that these initial conditions affect not only the growth rates, but also the asymptotic form of the vortex structures.

The effect of initial amplitude is a point of major importance which has not been adequately addressed up to now. In numerical computations of all types, it is convenient to start with relatively large initial amplitudes to save computation time. Conversely, in some experiments a strong initial distubance is used to isolate a specific wavelength from the continuous spectrum of background disturbances. We have shown that caution must be exercised in this approach if the results are to be interpreted as representative of infinitesimal disturbances. Finally, we note that disturbances in real flows may indeed be of finite amplitude, e.g. when a disturbance is introduced by convection from a distant part of the flow field.

The response of the vortex layer as a function of layer thickness (or wavelength) is a second area which requires careful consideration. Most calculations employing vortex markers cannot address this issue, because the layer is typically only a few markers thick. The subtle differences discovered in this paper require a resolution of small scales which is difficult to achieve with discrete vortex markers, except at prohibitive cost. Finite-difference calculations (Corcos & Sherman 1984) have examined different thicknesses, but only for a few cases. Moreover, the relatively low Reynolds numbers considered lead to the rapid diffusion of vorticity, effectively eliminating many of the thin layers studied in the present effort. We view our calculations as being complementary to the finite-difference solutions. On the one hand, we are showing fine details which are obscured in the viscous calculations, while, on the other, our inviscid results are not as easy to compare with experiments, because they represent the asymptotic limit of infinite Reynolds number. Taking the two sets of calculations together presents a more complete picture of vortex roll-up in real shear layers.

The lack of viscous dissipation just mentioned is one of the limitations of the present method. There are a number of other limitations which must now be examined. First and most obvious is the restriction to periodic layers with a single monochromatic disturbance. Other authors have discussed the imperfect analogy between the temporal growth of periodic disturbances and the spatial growth in a real shear layer (see e.g. Aref 1983 or Corcos & Sherman 1984); it is unnecessary to repeat those comments here. Of more direct concern is the restriction to a single-wavelength disturbance, which explicitly eliminates the possibility of vortex pairing – one of the most important growth mechanisms in real shear layers. There are three stages in the growth of disturbances on free shear layers: (1) exponential growth described by linear theory, (2) nonlinear growth leading to asymptotic configurations and (3) subharmonic interactions leading to vortex pairing. Previous calculations by authors mentioned above have modelled all three aspects of the growth process. We have restricted our calculations to the first two stages, in order that we might concentrate on the details of the nonlinear growth phase. We have stressed the differences in the asymptotic states of the various monochromatic disturbances precisely because vortex pairing is so important. Our final configurations form the initial conditions for subharmonic disturbances. Subtle changes in these base flows can lead to drastic differences in the further evolution of the layer as it undergoes vortex pairing. This subject will be dealt with further in a future paper.

We have dealt with the assumptions of inviscid flow and periodic disturbances. A final question concerns the assumption of constant-vorticity layers. The velocity profile associated with this vorticity distribution is a close approximation of real flows over the centre of the layer but possesses an unphysical jump in the velocity gradient at the edge. This discontinuity does not affect the overall development of the flow but may lead to irregularities in a rigorous mathematical analysis. It has already been shown (Meiron, Baker & Orszag 1982; Higdon & Pozrikidis 1985) that the discontinuity in velocity across a vortex sheet may lead to a singularity after a finite time. Among other effects, this leads to infinite curvature at a point on the sheet. It is possible that similar problems may occur with the constant-vorticity model. Fortunately, such occurrences would have a much weaker effect than in the case of vortex sheets. A final resolution of this question must await a more refined mathematical analysis.

Appendix

In this Appendix, we present the linear-stability theory for a constant-vorticity layer, following Rayleigh (1880). We consider an unperturbed shear layer with constant vorticity, such that

$$u = \left\{ \begin{array}{ll} U & (y > \frac{1}{2}b), \\ \dfrac{2U}{b} y & (-\frac{1}{2}b < y < \frac{1}{2}b), \\ -U & (y < -\frac{1}{2}b). \end{array} \right\} \tag{A 1}$$

The upper and lower boundaries of the vortex layer are perturbed such that

$$y^+ = \tfrac{1}{2}b + \eta_1, \tag{A 2}$$

$$y^- = -\tfrac{1}{2}b + \eta_2, \tag{A 3}$$

where

$$\eta_1 = \epsilon \, \mathrm{e}^{\mathrm{i}(kx - \sigma t)}, \tag{A 4}$$

$$\eta_2 = \epsilon \, \mathrm{e}^{\mathrm{i}(kx - \sigma t + \phi)}. \tag{A 5}$$

In these expressions, $\mathrm{Im}\,(\sigma)$ is the growth rate and ϕ is the phase angle.

The fluid velocity field may be written as a contour integral over the vortex region:

$$\boldsymbol{u}(\boldsymbol{x}) = -\frac{\omega}{2\pi} \int_C \ln |\boldsymbol{x} - \boldsymbol{x}'| \, \mathrm{d}l', \tag{A 6}$$

where the vorticity ω is just $-2U/b$.

The linearized kinematic conditions at the boundaries of the vortex layer require

$$U \frac{\partial \eta_1}{\partial x} + v = \frac{\partial \eta_1}{\partial t} \quad \text{at } y = y^+, \tag{A 7}$$

$$-U \frac{\partial \eta_2}{\partial x} + v = \frac{\partial \eta_2}{\partial t} \quad \text{at } y = y^-. \tag{A 8}$$

An expression for the disturbance velocity v is obtained by evaluating the contour integral (A 6) over the disturbed boundaries.

To leading order, this gives

$$v = -\tfrac{1}{2}\mathrm{i}\omega\eta_1 [1 - \mathrm{e}^{-kb + \mathrm{i}\phi}] \quad \text{at } y = y^+, \tag{A 9}$$

$$v = -\tfrac{1}{2}\mathrm{i}\omega\eta_2 [\mathrm{e}^{-kb - \mathrm{i}\phi} - 1] \quad \text{at } y = y^-. \tag{A 10}$$

Substituting for v in (A 7) and (A 8), yields the equations

$$kb + \frac{2\sigma}{\omega} = 1 - \mathrm{e}^{-kb + \mathrm{i}\phi}, \tag{A 11}$$

$$kb - \frac{2\sigma}{\omega} = 1 - \mathrm{e}^{-kb - \mathrm{i}\phi}, \tag{A 12}$$

which must be satisfied for non-zero η_1 and η_2.

Solving for σ and ϕ yields

$$\frac{2\sigma}{\omega} = \pm \mathrm{i} \, [\mathrm{e}^{-2kb} - (kb - 1)^2]^{\frac{1}{2}}, \tag{A 13}$$

$$\mathrm{e}^{\mathrm{i}\phi} = \mathrm{e}^{kb} \left[1 - kb - \frac{2\sigma}{\omega} \right]. \tag{A 14}$$

For values of the wavenumber in the range $0 < kb < 1.2785$, σ is purely imaginary, and the disturbance grows exponentially. The phase angle ϕ corresponding to the exponentially growing and decaying modes may be obtained from (A 14).

REFERENCES

ACTON, E. 1976 The modelling of large eddies in a two-dimensional shear layer. *J. Fluid Mech.* **76**, 561–592.

AREF, H. 1983 Integrable, chaotic and turbulent vortex motion in two-dimensional flows. *Ann. Rev. Fluid Mech.* **15**, 345–389.

AREF, H. & SIGGIA, E. D. 1980 Vortex dynamics of the two dimensional turbulent shear layer. *J. Fluid Mech.* **100**, 705–737.

ASHURST, W. T. 1979 Numerical simulation of turbulent mixing layers via vortex dynamics. In *Turbulent Shear Flows* I (ed. F. Durst *et al.*), pp. 402–413. Springer.

BIRKHOFF, G. 1962 Helmholtz and Taylor instability. *Proc. Symp. Appl. Math. Am. Math. Soc.* **13**, 55–76.

BREIDENTHAL, R. 1981 Structure in turbulent mixing layers and wakes using a chemical reaction. *J. Fluid Mech.* **109**, 1–24.

CORCOS, G. M. & SHERMAN, F. S. 1976 Vorticity concentration and the dynamics of unstable shear layers. *J. Fluid Mech.* **73**, 241–264.

CORCOS, G. M. & SHERMAN, F. S. 1984 The mixing layer: deterministic models of a turbulent flow. Part 1. Introduction and the two-dimensional flow. *J. Fluid Mech.* **139**, 29–65.

DEEM, S. G. & ZABUSKY, N. J. 1978 Vortex waves: stationary 'V states', interactions, recurrence and breaking. *Phys. Rev. Lett.* **40**, 859–862.

GEAR, C. W. 1971 *Numerical Initial Value Problems in Ordinary Differential Equations.* Prentice Hall.

HIGDON, J. J. L. & POZRIKIDIS, C. 1985 The self-induced motion of vortex sheets. *J. Fluid Mech.* **150**, 203–231.

HO, C. M. & HUERRE, P. 1984 Perturbed free shear layers. *Ann. Rev. Fluid Mech.* **16**, 365–424.

KIRCHHOFF, G. R. 1876 *Mechanik.* Leipzig: B. G. Teubner.

KRASNY, R. 1984 Ph.D. dissertation. University of California, Berkeley.

LAMB, H. 1932 *Hydrodynamics.* Dover.

LOVE, A. E. H. 1894 On the stability of certain vortex motions. *Proc. Lond. Math. Soc. Ser. 1* **25**, 18–43.

MEIRON, D. I., BAKER, G. R. & ORSZAG, S. A. 1982 Analytical structure of vortex sheet dynamics. Part 1. Kelvin–Helmholtz instability. *J. Fluid Mech.* **114**, 283–298.

OVERMAN, E. A. & ZABUSKY, N. J. 1982 Evolution and merger of isolated vortex structures. *Phys. Fluids* **25**, 1297–1305.

PIERREHUMBERT, R. T. & WIDNALL, S. E. 1981 The structure of organized vortices in a free shear layer. *J. Fluid Mech.* **102**, 301–313.

PULLIN, D. I. 1981 The nonlinear behaviour of a constant vorticity layer at a wall. *J. Fluid Mech.* **108**, 401–421.

RAYLEIGH, LORD 1980 On the stability or instability of certain fluid motions. *Proc. Lond. Math. Soc.* **xi**, 57–70.

SAFFMAN, P. G. & SZETO, R. 1980 Equilibrium shapes of a pair of equal uniform vortices. *Phys. Fluids* **23**, 2339–2342.

SAFFMAN, P. G. & SZETO, R. 1981 Structure of a linear array of uniform vortices. *Stud. Appl. Math.* **65**, 223–248.

ZABUSKY, N. J., HUGHES, M. H. & ROBERTS, K. V. 1979 Contour dynamics for the Euler equations in two dimensions. *J. Comp. Phys.* **30**, 96–106.